Progress in Materials Science 92 (2018) 225–257

Contents lists available at ScienceDirect

Progress in Materials Science

journal homepage: www.elsevier.com/locate/pmatsci

# A literature review of Ti-6Al-4V linear friction welding

Anthony R. McAndrew [b,c,*], Paul A. Colegrove [a], Clement Bühr [a], Bertrand C.D. Flipo [c], Achilleas Vairis [d]

[a] Cranfield University, Cranfield, Bedfordshire MK43 0AL, UK
[b] Cranfield University, Cranfield, Bedfordshire MK43 0AL, UK[1]
[c] TWI Ltd, Granta Park, Great Abington, Cambridge CB21 6AL, UK
[d] Technological and Educational Institute (TEI) of Crete, Heraklion 71004, Greece

ARTICLE INFO

*Article history:*
Received 16 January 2017
Received in revised form 21 May 2017
Accepted 11 October 2017
Available online 25 October 2017

*Keywords:*
Linear friction welding
Titanium alloy
Literature review
Ti64
Ti6Al4V
Microstructure
Mechanical properties
Modelling
Residual Stress
Energy
Advantages

ABSTRACT

Linear friction welding (LFW) is a solid-state joining process that is an established technology for the fabrication of titanium alloy bladed disks (blisks) in aero-engines. Owing to the economic benefits, LFW has been identified as a technology capable of manufacturing Ti-6Al-4V aircraft structural components. However, LFW of Ti-6Al-4V has seen limited industrial implementation outside of blisk manufacture, which is partly due to the knowledge and benefits of the process being widely unknown. This article provides a review of the published works up-to-date on the subject to identify the "state-of-the-art". First, the background, fundamentals, advantages and industrial applications of the process are described. This is followed by a description of the microstructure, mechanical properties, flash morphology, interface contaminant removal, residual stresses and energy usage of Ti-6Al-4V linear friction welds. A brief discussion on the machine tooling effects is also included. Next, the work on analytical and numerical modelling is discussed. Finally, the conclusions of the review are presented, which include practical implications for the manufacturing sector and recommendations for further research and development. The purpose of this article is to inform industry and academia of the benefits of LFW so that the process may be better exploited.


**Contents**



* Corresponding author at: TWI Ltd, Granta Park, Great Abington, Cambridge CB21 6AL, UK.
*E-mail address:* anthony.mcandrew@twi.co.uk (A.R. McAndrew).
[1] Formerly.

https://doi.org/10.1016/j.pmatsci.2017.10.003
0079-6425/

## 1. Introduction

Linear friction welding (LFW) is a solid-state joining process that works by oscillating one workpiece relative to another while under a large, compressive force; see Fig. 1(a). The friction between the oscillating surfaces produces heat which causes the interface material to plasticise. The plasticised material is then expelled from the interface causing the workpieces to shorten (burn-off) in the direction of the compressive force [1–4]. During the burn-off the interface contaminants, such as oxides and foreign particles, which can affect the properties [5,6] and possibly the service life of a weld [7], are expelled from

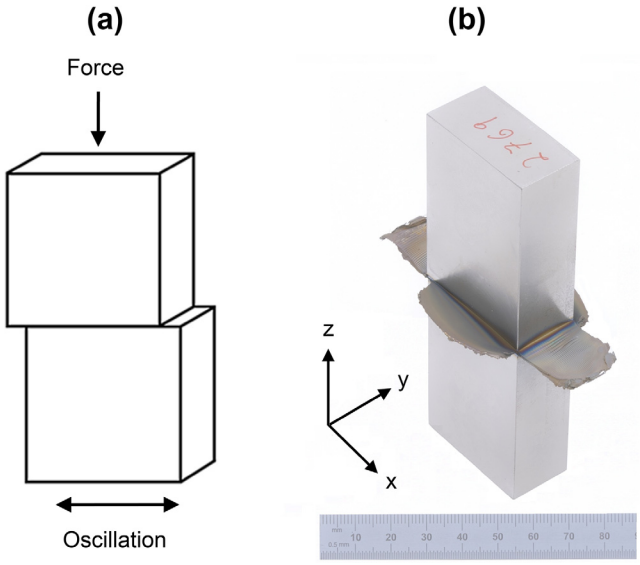


**Fig. 1.** (a) **LFW process schematic and (b) a completed Ti-6Al-4V weldment showing the expelled interface material (flash), where the oscillatory motion occurred in the 'x' direction** [16].

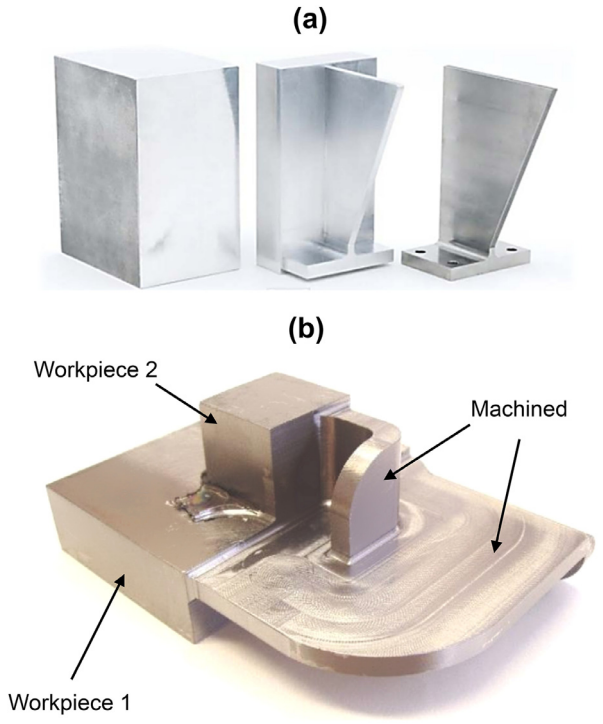


**Fig. 2.** (a) An aerospace component machined from an oversized block of metal (image courtesy of TWI [25]), and (b) A Ti-6Al-4V preform fabricated using the LFW process - the as-welded structure can be seen on the left side of the figure and the final machined component on the right (image courtesy of TWI [1]).

the weld into the flash [8]. Once free from contaminants, pure metal to metal contact occurs resulting in an integral bond [8–16]. Fig. 1(b) shows an example of a completed weld.

LFW is an established technology for the manufacture of titanium alloy integrated bladed disks (blisks) for aero-engines [2,8,17–19]. However, owing to the many benefits of the process, it is finding increasing interest for the manufacture of aircraft structural components – particularly for Ti-6Al-4V. This is primarily owing to titanium and its alloys being extremely expensive in terms of purchase cost (>£70 $kg^{-1}$), energy consumption (>500 $MJ{\cdot}kg^{-1}$) and $CO_2$ emissions (>40 $kg{\cdot}kg^{-1}$) [20]. Typically, Ti-6Al-4V aircraft structural components are machined from oversized ingots, forgings and extrusions [21]. This is an expensive process due to the proportionally large amount of material that is purchased compared to the amount that remains after machining [22,23]; see Fig. 2(a). The buy-to-fly (BTF) ratios of components manufactured using this approach can be as poor as 20:1 and are rarely as low as 5:1 [21,23]. LFW reduces the material required to make a component by joining smaller workpieces to produce a preform, which is subsequently machined to the desired dimensions, as shown in Fig. 2(b). This brings substantial improvements to the BTF ratios, which significantly reduces manufacturing costs [1,2,8,24]. For example, BTF ratios as low as 2:1 and 1.6:1 have been quoted for components machined from linear friction welded Ti-6Al-4V preforms [21,25]. The linear friction welded components also have a comparable strength and quality to machined parts [26]. Preliminary investigations suggest that up to 50% of all titanium alloy aerospace structures can be manufactured using the LFW process [21].

Despite the interest, LFW of Ti-6Al-4V has experienced limited industrial implementation outside of blisk manufacture. This is partly due to the knowledge and benefits of the process being widely unknown. A significant amount of academic and industrial research has been conducted in recent years [27]. The purpose of this article is to provide an up-to-date review of the published works on the linear friction welding of Ti-6Al-4V so that the current "state-of-the-art" may be identified and the process better exploited. The order of the review is as follows: First, the LFW process background, fundamentals, advantages and industrial applications are discussed. Second, the microstructure, mechanical properties, flash morphology, interface contaminant removal, residual stresses and energy usage of Ti-6Al-4V linear friction welds are presented, a brief discussion on the machine tooling effects is also included. Next, the work on process modelling is discussed. Finally, the conclusions of the review are presented, which include practical implications of the article findings for the manufacturing sector and recommendations for further research.

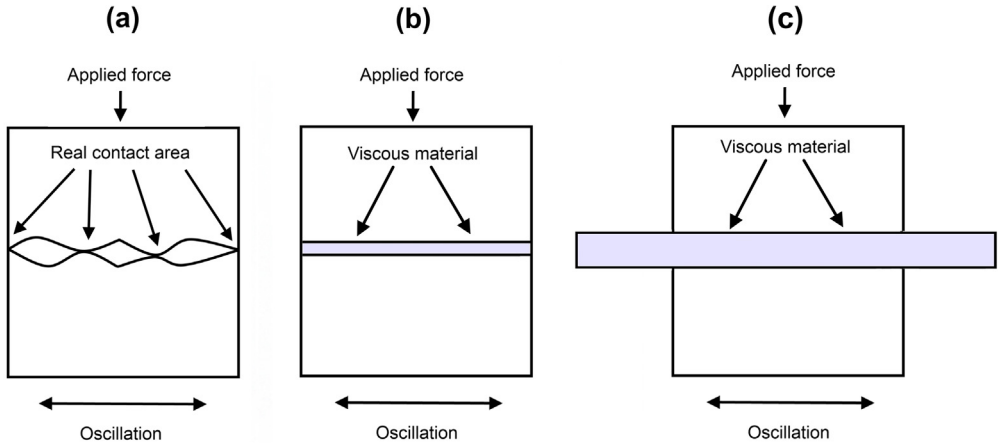


**Fig. 3.** (a) **asperity interaction (Phase 1), (b) viscous material formation (Phase 2), and (c) steady-state condition showing the expelled interface material (Phase 3)** [14,15].

## 2. Background and process fundamentals

### *2.1. Background*

The linear friction welding process was first patented in the late 1920s [8], however there was very little detail recorded on its use. A discussion of the process was then recorded in the USSR in the 1960s [28], but it was described as being "very doubtful" as a manufacturing technique [8,28] due to the difficulty in generating reciprocating linear motion [28]. The first real structured industry research into the process took place at TWI, UK in the 1980s [2], while the first recorded academic research took place at Ohio State University, USA [9,29] and the University of Bristol, UK [3,30–33]. When compared to other friction welding processes, where there are numerous published works, there has been relatively little information available on LFW until recently [1,3,10].

### *2.2. Process phases*

As previously stated, linear friction welding (LFW) is a solid-state joining process that works by oscillating one workpiece relative to another while under a large, compressive force, as shown in Fig. 1(a). Despite being one continuous process, LFW is said to occur over four phases [3,31]:

- Phase 1 – Initial phase. Microscopic contact exists between asperities on the two surfaces to be joined and heat is generated due to friction; see Fig. 3(a). The asperities soften and deform, increasing the true area of contact between the workpieces. Negligible axial shortening (burn-off) in the direction of the applied force is observed during this phase.
- Phase 2 – Transition phase. The heat due to friction causes the interface material to plasticise and become highly viscous, as shown in Fig. 3(b). This causes the true area of contact between the workpieces to increase to 100 percent of the cross-sectional area. Heat conducts away from the interface, softening more material, and burn-off begins to occur due to the expulsion of the viscous material from the interface. For the Ti-6Al-4V alloy, this phase begins when the interface reaches the β-transus temperature [15].
- Phase 3 – Equilibrium phase. A quasi-steady-state condition is achieved and the axial shortening (burn-off) occurs at a nearly constant rate through the rapid expulsion of the viscous interface material, forming the flash; see Fig. 3(c)
- Phase 4 – Deceleration and forging phase. The relative motion is ceased and the workpieces are aligned. In some applications an additional increased forging force may be applied to help consolidate the weld.

### *2.3. Process parameters*

There are eight process parameters used during linear friction welding [1–3,6–8,16,34–45]:

- Oscillation frequency
- Oscillation amplitude
- Applied force/Normal force
- Burn-off/Axial shortening/Upset
- Ramp-up time (time taken for the amplitude and frequency to reach a steady-state level)

- Oscillation decay time (time taken to decay the amplitude and frequency to a stop)
- Forging force (the force used to help consolidate the weld post-oscillatory motion)
- Forging force time (the time the forging force is applied)

Many authors appear to consider the frequency, amplitude, applied force and burn-off to be the process inputs of primary importance [2,3,6,46–50]. Although the frequency and amplitude of oscillation are two separate process inputs it has been shown in several cases that they may be considered as a single input – an average rubbing velocity – as varying either while keeping the average rubbing velocity constant has relatively little effect on the results for Ti-6Al-4V linear friction welds [14–16]. The average rubbing velocity ($v_r$) is defined as [1]:

$$v_r = 4 \cdot Amplitude \cdot frequency \tag{1}$$

### 2.4. Process advantages and limitations

Linear friction welding offers many advantages over competing manufacturing processes, for example:

- The weld remains in the solid-state, avoiding many of the defects associated with melting and solidification during fusion welding [11,42,51–56], such as pores and solidification cracks. The distortion of the welded component is also reduced [10,40,57–60]
- The process has lower peak temperatures than fusion welding, reducing intermetallic formation and allowing for a range of dissimilar materials to be joined [43,45,61–64]
- The process does not need a filler metal, flux and shielding gas [10]
- The process is easily automated, making the process highly repeatable and not dependant on human influence [1,2,49], resulting in very low defect rates [15]
- When used to fabricate preforms the material usage and manufacturing costs are reduced when compared to subtractive techniques (e.g. CNC machining) [1,2,8]

The process does however have some limitations, for example:

- The cost and size of the machines
- The maximum weld size is limited by the size of the machine and is typically limited to several hundred millimetres square

## 3. Industrial usage of LFW

### 3.1. Bladed disk (Blisk) manufacturing

In general, the LFW process is considered to be an "exotic" technology for the manufacture of high-value aerospace components [1,2]. This is primarily due to the expensive cost of the first generation equipment and the fact that most industrial LFW machines are owned by aerospace manufacturers [2].

To date, the process is commercially established as a technology for the fabrication of titanium alloy integrated bladed disks (blisks) in aero-engines [2,8,17–19,27,65]. Titanium blisks are used in low temperature sections of aero-engines. Typically, Ti-6Al-4V (Ti-64) is used for applications up to 300 °C and Ti-6Al-2Sn-4Zr-2Mo-0.15Si (Ti-6242) for applications up to 480 °C [4,66]. Rolls Royce, MTU Aero Engines, General Electric and Pratt & Whitney all use the LFW process to commercially produce titanium alloy blisks [4,67,68]. Fig. 4(a) shows an example of a blisk manufactured using the LFW process.

LFW offers many advantages when manufacturing blisks, for example conventionally manufactured bladed disk assemblies are reliant on mechanical fixings and dovetail joints to join the blade to the disk, as shown in Fig. 4(b). LFW allows for the blade to be integrally joined to the disk which significantly reduces the weight of the component [4,47,69], even by as much as 30% [4,47]; see Fig. 4(c). In addition to the weight savings, the lack of a mechanical interface between the blades and the disks eliminates common sources for fatigue crack initiation [4,66], which is often the life limiting feature of these parts [4]. This can result in extended inspection intervals [66]. Furthermore, linear friction welded blisks also have improved performance (e.g. better aerodynamics), which reduces the operating costs for the end user [7,18,35,44,58,70].

Another alternative to using mechanical fixings is to machine the blisk from a solid block [4,71,72]. When compared to the LFW process this is a costly exercise due to the amount of waste material generated – particularly for larger blisks [7,66]. Blisks machined from a solid block must comprise of a single material [4,71]. Linear friction welding has the advantage of joining disks and blades of different materials [4,71].

### 3.2. Future concepts

As discussed in the Section 1, in addition to blisk manufacture, there is an industrial interest to use LFW to produce a wide range of structural aerospace preforms [13,50], such as those shown in Fig. 2(b) and Fig. 5. This is primarily due to the

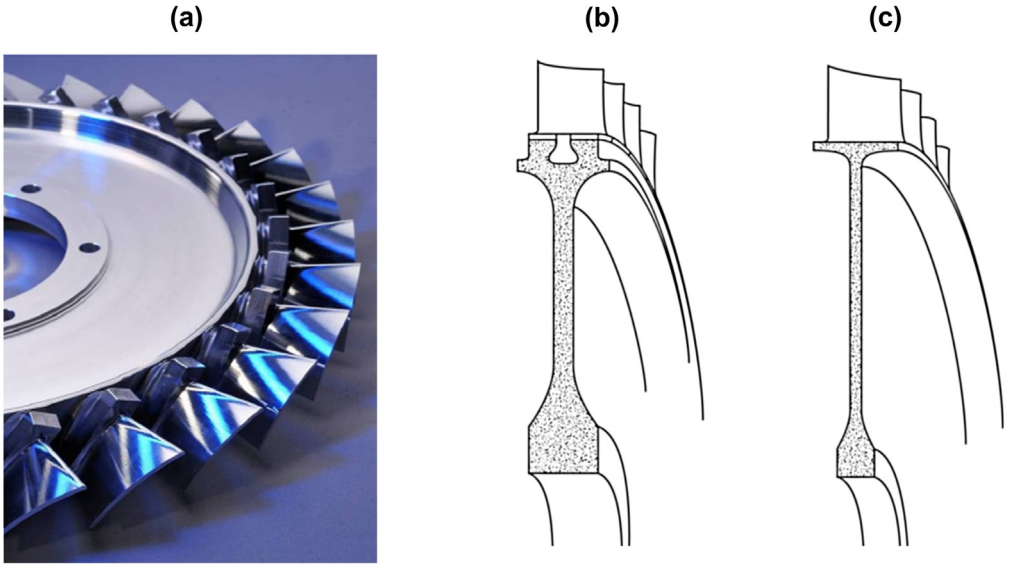


**Fig. 4.** (a) an integrated bladed disk (blisk) manufactured at TWI (image courtesy of TWI), (b) a conventional bladed disk assembly [7] and (c) a linear friction welded blisk [7].

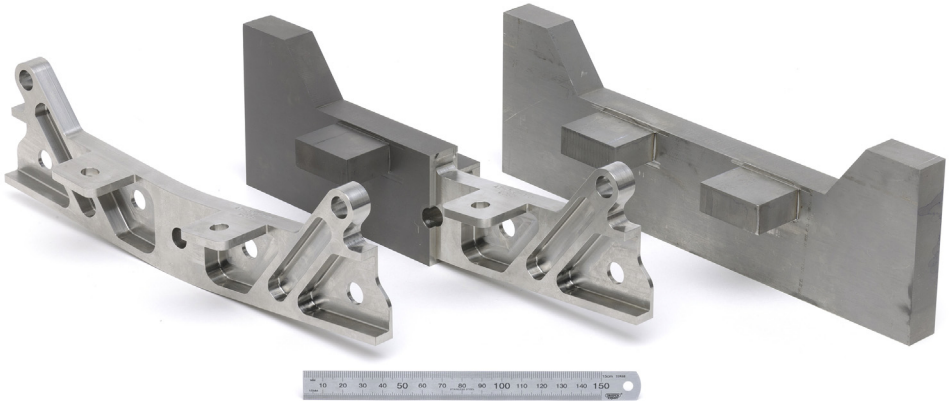

**Fig. 5.** Demonstration of an aerospace structural component being machined from a linear friction welded Ti-6Al-4V preform (Image courtesy of TWI and the TiFab Consortium [21]).

significant cost savings that can be achieved. For example, when compared to machining from block, material cost savings of up to 90% can be obtained [1,25,27] and the estimated *total* manufacturing cost of a component can be reduced by 23–80% [21,73,74].

In addition to joining workpieces with a single surface of contact, as shown for the components in Figs. 1(b), 2(b) and 5, there is an industrial need to join non-planar surfaces to better enable the manufacture of complex structural preforms [27,50,75,76]; see Fig. 6(a) and (b). For example, The Boeing Company is interested in the joining of a "keystone" workpiece to two flanges and a base plate [75], as shown in Fig. 6(c). The flanges are welded to the base plate first (stage 1 weld) and the generated flash removed and the surfaces re-cleaned. The stage 1 welds are straight forward as only one surface is required to be joined to the base plate. However, production of the "bridging weld" (stage 2 weld) where the keystone workpiece is joined to the assembly might be problematic as there are multiple surfaces that need to be welded concurrently.

### 3.3. LFW machine manufacturers

As far as the authors can tell, there are five major LFW machine manufacturers: ACB (France), APCI (Indiana, USA), KUKA Systems (Germany), MTI (Indiana, USA) and Thompson Friction Welding (UK). On a basic level LFW machines work by oscillating one workpiece relative to another while under a large, compressive force. According to Bhamji [65], the force

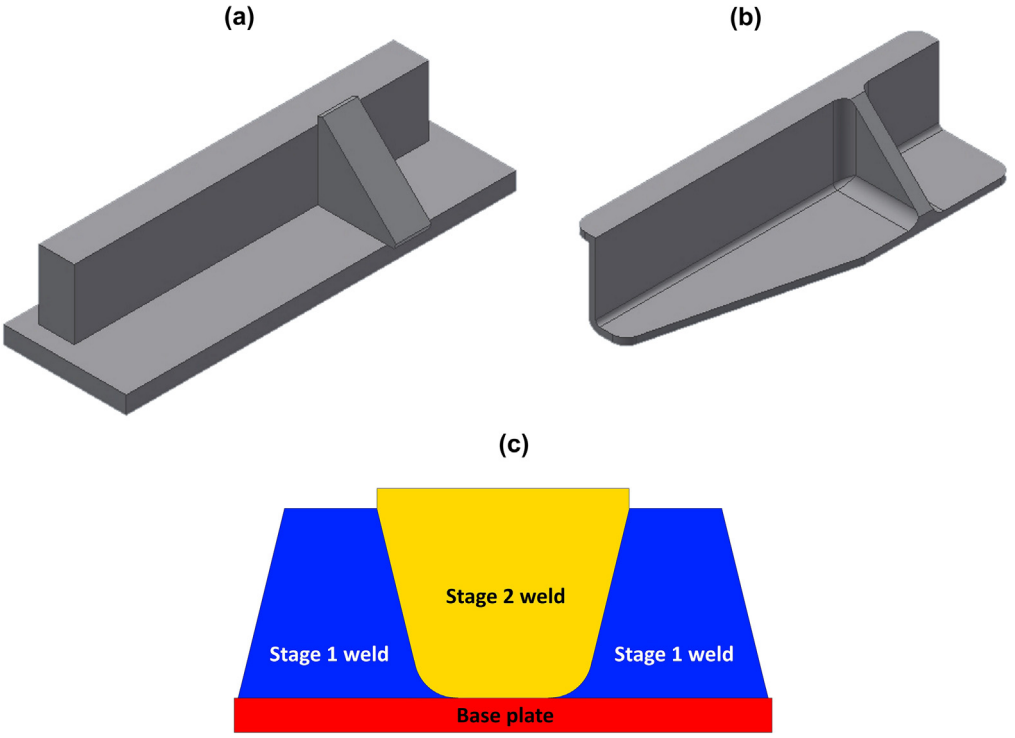


**Fig. 6.** Linear friction welding of non-planar surfaces, showing: (a) an illustration of a preform, (b) an illustration of the component machined from (a), and (c) the manufacturing process of the "keystone" weld where the oscillations occur in and out of the viewing plane.

application is always generated by a hydraulic ram, while the oscillatory motion can be generated mechanically or hydraulically, as shown in Fig. 7(a) and (b), respectively.

Mechanically operated systems often use a motor to rotate a crankshaft. Attached to the crankshaft are two cranks that can be phase shifted. A whipple beam is attached to the cranks. When the cranks are 180° out of phase the beam rotates around its centre point causing the centre to remain stationary, which effectively gives an oscillation amplitude of zero. To achieve oscillation amplitudes between zero and the maximum, the phase shift is altered between 0° and 180° [2,65]. The frequency is dependent on the revolutions per minute of the motor [2]. The tooling that holds the workpieces is attached to the centre of the whipple beam. Hydraulic operating systems work by pumping high pressure fluid into a stack of accumulators (tanks). A servo valve then allows the high pressure fluid from the accumulators to be alternated between each end of a cylinder. This oscillates a piston at a desired amplitude and frequency. The tooling that holds the workpiece to be welded is attached to the end of the piston.

LFW machines are capable of delivering the dimensional precision, with high repeatability, required by the aerospace industry. For example, the TiFab consortium demonstrated a positional tolerance value of ±0.025 mm for the process [21] and the IHI corporation showed that the angular variance for a welded component was as low as 0.04° [78].

Recently, the TiFab consortium demonstrated that 95% of all titanium alloy aerospace components suitable for manufacturing by LFW can be produced using a machine with a maximum applied force of 50 tonnes [79].

## 4. Ti-6Al-4V linear friction welds

The LFW process is typically used for joining metals, however, it has been used to join plastics [80,81] and wood [82,83]. LFW is particularly effective for joining metals that have good high-temperature properties, i.e. compressive yield and shear strength, and low thermal conductivities [1,8]. This allows for the generated heat to remain at the interface causing the interface to rapidly heat and plasticise. This makes titanium alloys particularly suitable for the process, however many similar and dissimilar material combinations have also been investigated with varying degrees of success [1,2,4,5,8,29,36,38,40,43,45,49,57,60,61,63,64,66,67,84–103]. As the focus of this review is on the titanium alloy Ti-6Al-4V, the remainder of this section will focus on the microstructure, mechanical properties, flash morphology, interface contaminant removal, residual stresses and energy usage of Ti-6Al-4V linear friction welds. The effects of the machine tooling and processing conditions on these responses are also discussed.

Ti-6Al-4V is an $\alpha$+$\beta$ alloy that was developed in the 1950s at the Illinois Institute of Technology, USA [66]. The alloy is known for its excellent strength to weight ratio. It is the most commonly used titanium alloy - approximately 50% of all

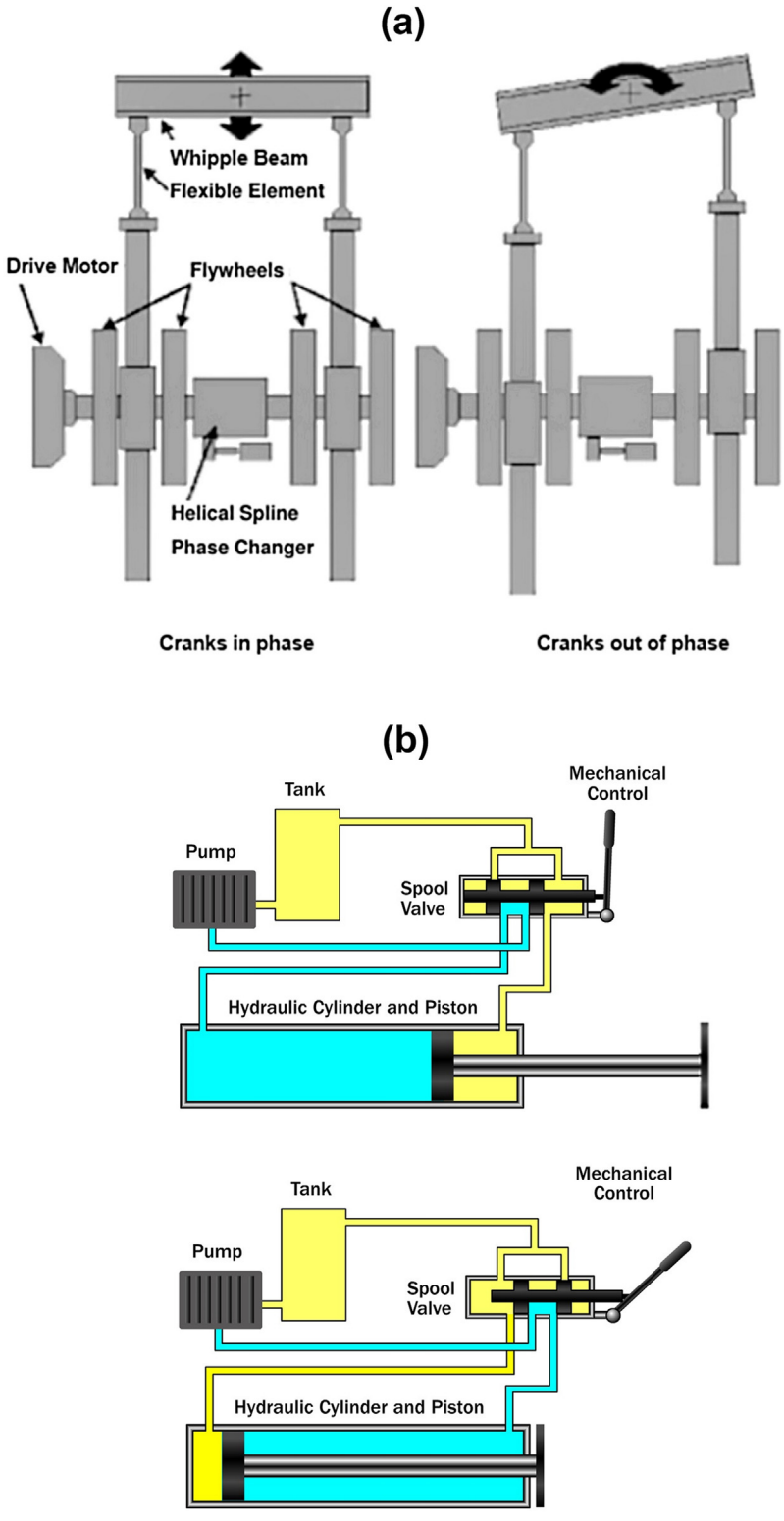


**Fig. 7.** Schematic of (a) mechanically operated motion (image courtesy of TWI [2]) and (b) hydraulically operated motion [77].

titanium alloys used are of this composition [58,66]. However, the material is comparably expensive to other metals, hence its interest for LFW. The Ti-6Al-4V alloy consists of approximately 6% aluminium, which stabilises the α phase, and 4% vanadium, which stabilises the β phase [104,105]. The β phase constitutes ten percent by volume fraction at room temperature

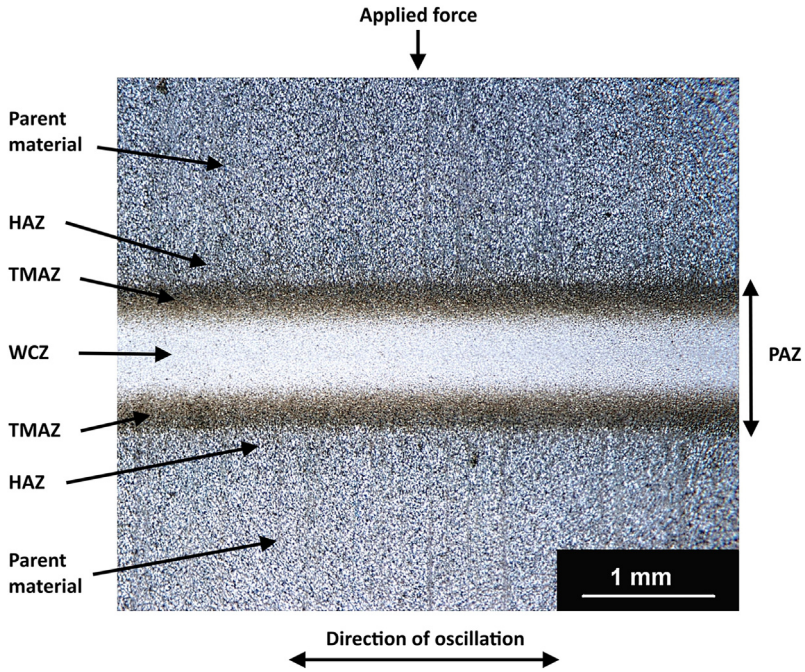


**Fig. 8.** Macroscopic section of a Ti-6Al-4V linear friction weld [15]

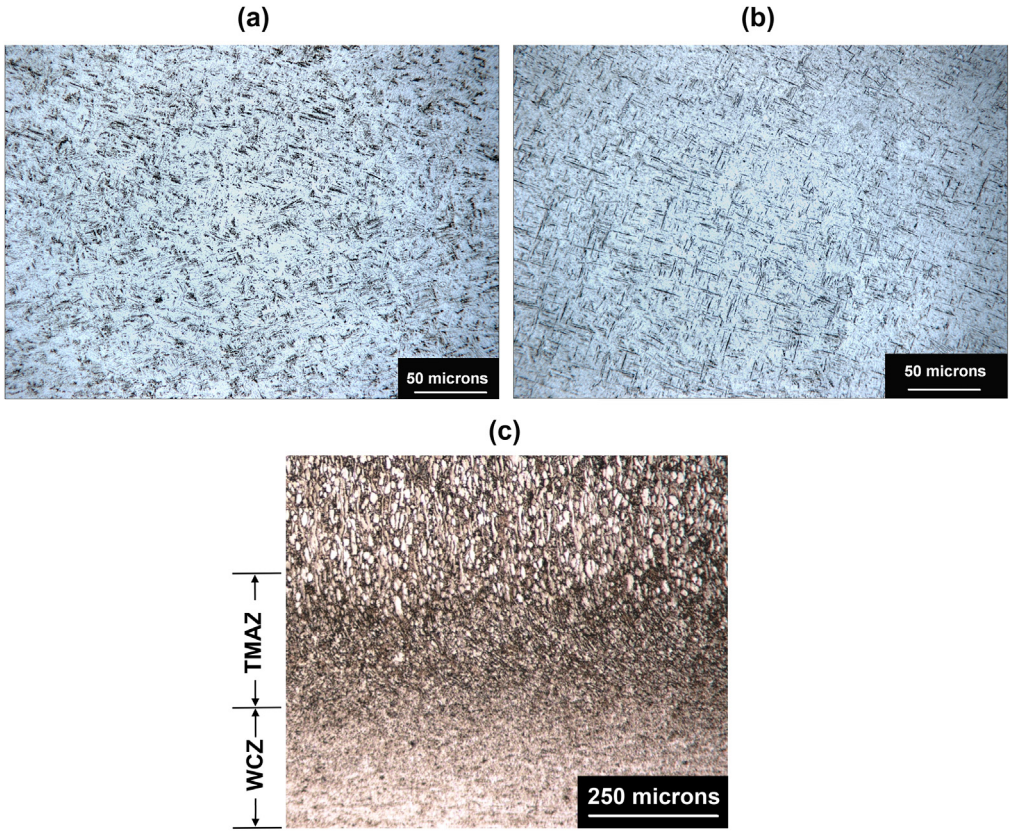


**Fig. 9.** (a) Widmanstatten [15], (b) Martensite [15], and (c) TMAZ [13].

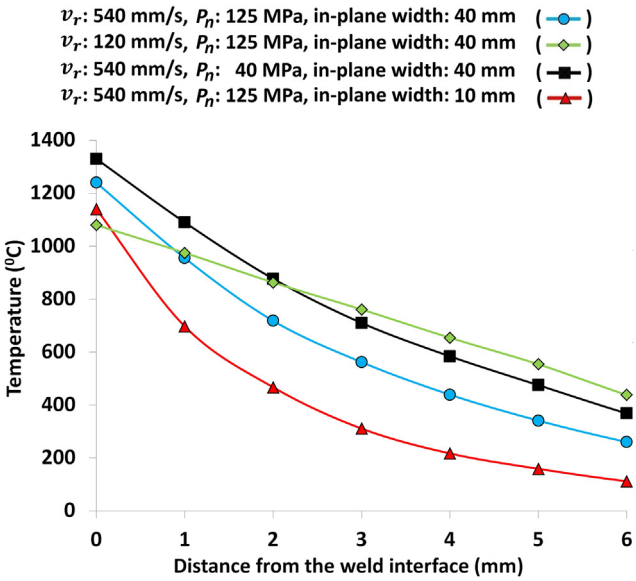


**Fig. 10.** Thermal profiles in Ti-6Al-4V linear friction welds showing the effects of the rubbing velocity, $v_r$, pressure, $P_n$, and in-plane width. These profiles were obtained from FEA [13,14].

[106]. Ti-6Al-4V is commercially produced to have one of three types of microstructure [69]. These are fully lamellar, fully equiaxed and bi-modal. Each type has its own benefits and draw backs. It should be noted that the wrought Ti-6Al-4V typically used in the literature for the linear friction welding process, where reported, tends to be of the bi-modal microstructure [6,13–15,34,35,41,44,53,56,58,70,71,107].

### 4.1. Microstructure and thermal observations

Regardless of the process inputs and geometry of the workpieces used the macrostructures of Ti-6Al-4V linear friction welds are similar in appearance in that they have several distinct zones: a weld centre zone (WCZ), a thermo-mechanically affected zone (TMAZ) and a heat affected zone (HAZ), and are surrounded by the flash [6,13–16,34,35,53]. A typical example of a weld is shown in Fig. 8. Technically the WCZ and the TMAZ are both "thermo-mechanically affected zones" but due to the vastly different microstructures they possess they are often considered separately [2,6,8,13,14,34,58]. The WCZ experiences *significant* dynamic recrystallisation (DRX), the TMAZ does not. The material in HAZ is not deformed mechanically but is affected by the heat. The region from one TMAZ/HAZ boundary to the other is often refered to as the "TMAZ thickness" or the plastically affected zone (PAZ) [13,14,18,108–110]. For the remainder of this article this region will be refered to as the PAZ.

The region of material that experiences the most significant change during the LFW process is the WCZ. The temperature at the interface surpasses that of the β-transus temperature [6,7,13,14,39,55,58,78] – 980 °C to 1010 °C depending on the quantities of the interstitial elements – transforming the α-grains into β-grains. The WCZ also experiences large strains and strain rates (up to 2500 $s^{-1}$) during processing [7,13,14], which results in significant dynamic recrystallisation of the high-temperature β-phase material [6,41,111,112]. The fully β-transformed microstructure cools rapidly after the oscillatory phases of the process, preventing β-grain coarsening, resulting in a Widmanstätten [6,8,13–15,18,34,56] or Martensitic [6,15,18,34,113] microstructure, as shown in Fig. 9(a) and (b), respectively. The difference, according to Ahmed and Rack [114], is due to the rate of cooling from the single β-phase. If the weld cools at a rate faster than 410 °C $s^{-1}$ a diffusionless transformation occurs resulting in Martensite; according to Karadge et al. [18] some metastable β-phase may also remain. If the weld cools at rate slower than 410 °C $s^{-1}$ then a diffusional transformation occurs resulting in a Widmanstätten morphology.

The majority of researchers suggest that the microstructure of the TMAZ does not reach the β-transus as fragments of the α-grains from the parent material are still present [6,18,35,55,58]. These grains tend to be deformed, elongated and re-orientated in the direction of oscillation [2,8,13–15,35,109]; see Fig. 9(c).

It should be noted that due to the structural stability of Ti-6Al-4V below temperatures of 800 °C [94,115] it is often difficult to detect a purely heat affected zone. However, a HAZ is more noticeable in welds that are produced with low rubbing velocities [16].

The extent of the PAZ and HAZ are very dependent on the processing conditions used. An increase of the amplitude and frequency (rubbing velocity) has been shown to reduce the extent of the HAZ while having a minimal effect on the PAZ. This is due to the effects of the rubbing velocity on the generated thermal profiles. As shown by comparing the blue and green lines in Fig. 10, the greater rubbing velocities increase the gradient of the thermal profile, reducing the extent of material

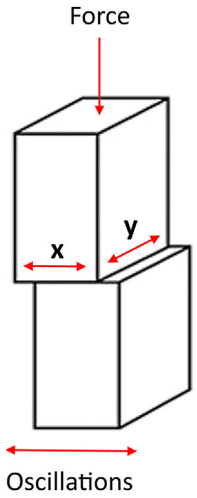


**Fig. 11.** An illustration of the workpiece dimensions, where 'x' is in the direction of the oscillations (in-plane width) and 'y' is out-of-plane to the oscillations.

above 800 °C. The increased thermal gradient is a consequence of the higher power input generated by the larger rubbing velocities, which causes the interface material to heat and plasticise more rapidly during phase 1, then shorten much more rapidly during phases 2 and 3. Therefore reducing the time the heat has to conduct away from the weld interface [15]. This may explain why HAZs are more noticeable with low rubbing velocities – a greater extent of the weld materials is above 800 °C therefore making the HAZ more observable to the naked eye [7,14,15,46,108]. Although the rubbing velocities have a big effect on the thermal profiles they have minimal effect on the extent of the PAZ [13,14,108]. McAndrew et al. [13–15] demonstrated that for noticeable material deformation to occur in Ti-6Al-4V linear friction welds the temperature of the material must approach the β-transus. As shown by comparing the blue and green lines in Fig. 10, despite the big difference in the thermal profiles, the extent of material at or above the β-transus is minimal, hence a minimal difference in the extent of the PAZ for different rubbing velocities. Furthermore, many authors agree that an increase of the rubbing velocity increases the interface temperature [7,13,14,46,108].

An increase of the pressure decreases the extent of the HAZ and PAZ [2,13,14,34,46,78,110]. This phenomenon can be explained by the effect of the pressure on the power input and burn-off rate. An increase of the pressure results in the burn-off rate being increased by a greater percentage than the power input [14]. Although more heat goes into the weld it is expelled at a faster rate. This decreases the time the heat has to conduct back from the interface, decreasing the extent of the HAZ and PAZ. Interestingly, this phenomenon also has an effect on the interface temperature. The material farther back from the interface is much cooler in welds produced with higher pressures, as shown by comparing the blue and black lines in Fig. 10. When this cooler material reaches the weld interface it effectively cools the weld producing a *lower* interface temperature [13–15,34,47,110]. According to Kuroki et al. [78] and Wanjara et al. [6] the α-phase lamella in the WCZ is increasingly refined when produced with larger applied forces. Moreover, Wanjara et al. [6] showed that an increase of the applied force increases the size of the DRX β-grains in the WCZ. This observation is in contrast to Attallah et al. [110], who for Ti-6246 welds showed that an increase of the applied force decreases the DRX β-grains in the WCZ. Consequently, the authors of this article believe the effects of the processing conditions on the microstructure need to be further investigated.

There is good agreement among authors on the effects of the workpiece geometry on the PAZ, HAZ and microstructure of Ti-6Al-4V linear friction welds [13,18,116,117]. Karadge et al. [18], for an identical combination of process inputs, showed that the post-weld interface grain size and the extent of the PAZ decreased when the workpiece dimension in the direction of oscillation ('x' in Fig. 11) was decreased; hereafter the 'x' value in Fig. 11 is referred to as the "in-plane width". McAndrew et al. [13,117] investigated the reasons for this phenomenon. In general, a reduction of the in-plane width increases the burn-off rate which results in rapid expulsion of the heated interface material [13,116,117]. This reduces the time the heat has to conduct back from the weld interface, reducing the extent of the material above the β-transus and therefore the PAZ, as can be seen by comparing the blue and red lines in Fig. 10. Moreover, a reduction of the in-plane width *decreases* the interface temperature for the same reason an increase of the pressure does [13,116,117]. The finer microstructure for the welds that were produced with the smaller in-plane widths could have been due to the higher strain rates experienced at these conditions [13]. This would have caused more recrystallisation during processing, refining the β-grains [112,115]. Furthermore, according to Gil et al. [118], the Widmanstätten morphology is finer with faster cooling rates. McAndrew et al. [13] showed that the post-oscillatory motion cooling rate can be dramatically increased when welds are produced with smaller in-plane widths. For example, for welds produced with 40 mm, 20 mm and 10 mm in-plane widths at an average rubbing velocity of 540 mm·s$^{-1}$ and a pressure of 125 MPa the centre of the weld interface cooled from the β-transus temperature to 500 °C at a rate of 110 °C s$^{-1}$, 210 °C s$^{-1}$ and 320 °C s$^{-1}$, respectively. This phenomenon was due to the narrower band of highly heated

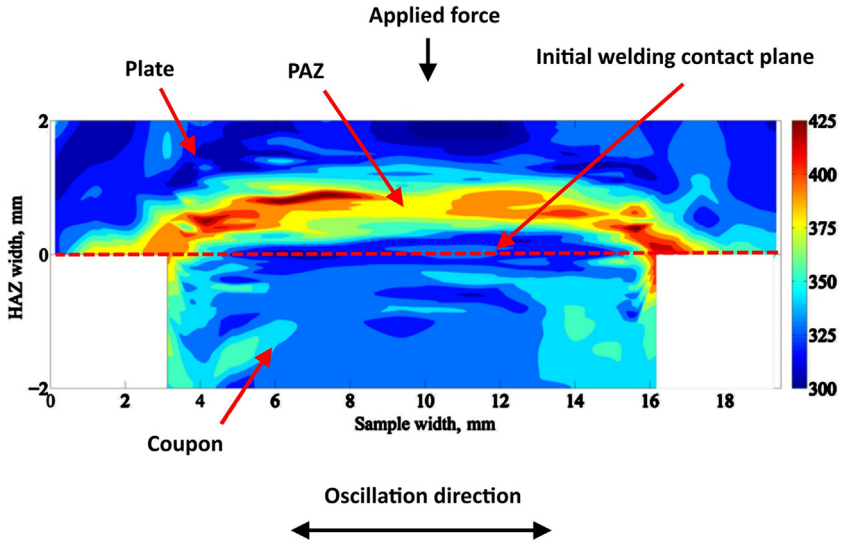


**Fig. 12.** Microhardness maps for a Ti-6Al-4V coupon to plate weld. Note that the harder regions correspond to the PAZ [116].

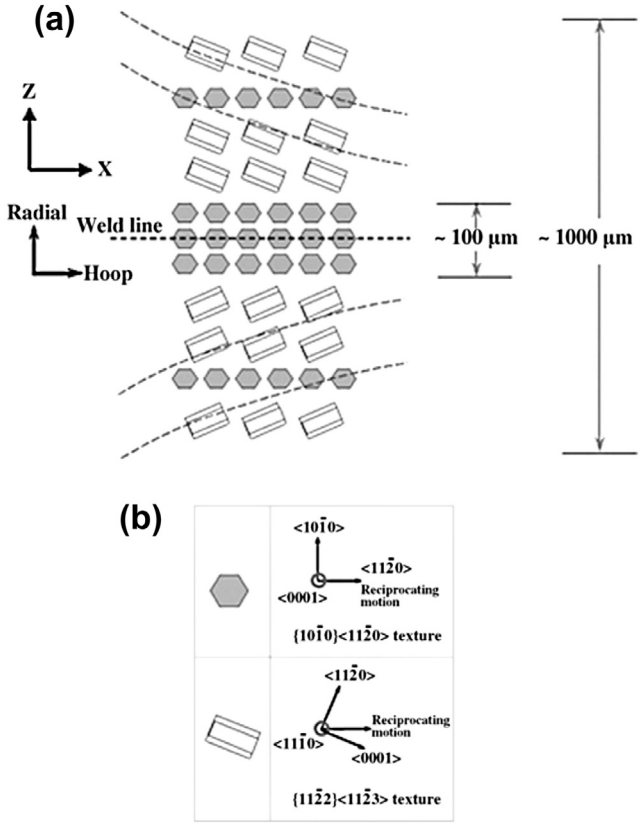


**Fig. 13.** (a) Crystallite orientation in the PAZ in a full-scale specimen, and (b) texture type [18].

material produced with smaller in-plane widths; see Fig. 10. The narrower band of heated material had less heat to be conducted from the interface region into the bulk material, allowing for a faster rate of cooling. The more refined WCZ microstructure for the welds produced with the smaller in-plane widths may, according to the literature, possess superior mechanical properties [58,119,120]. This observation suggests that there is a benefit to oscillating the workpieces along the shorter of the two interface contact dimensions as the temperature will be reduced and the mechanical properties improved

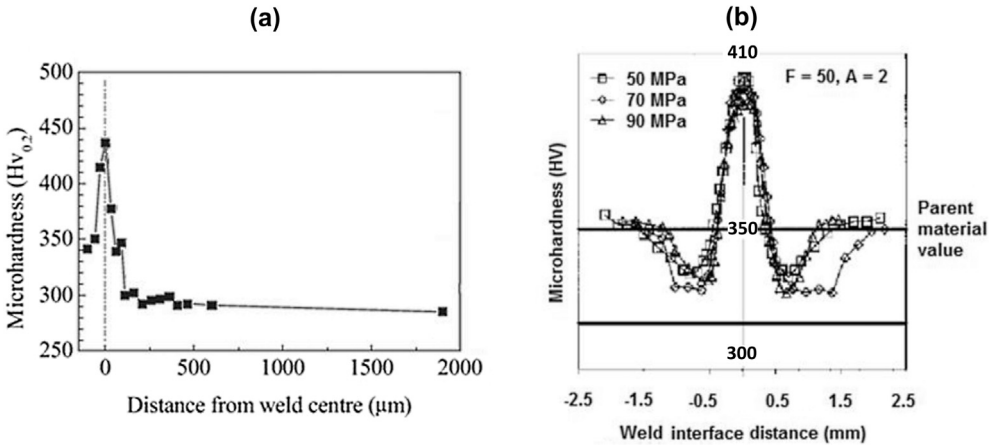


**Fig. 14.** TMAZ hardness: (a) higher than parent [53] and (b) lower than parent [6].

[13,117]. Worthy of note, the out-of-plane dimension ('y' in Fig. 11) has been shown to play little effect on the extent of the HAZ and PAZ, and microstructure [13,16,116].

To date, much of the academic research into LFW has been concerned with the joining of workpieces with identical contacting surface dimensions [3,13–15,18,24,34,35,48,53,58,107,110,121,122]. These geometries tend to generate a PAZ and HAZ that are symmetric around the weld interface. There is an industrial interest to understand the joining of dissimilar sized workpieces. To address this issue, Astarita et al. [123], Schroeder et al. [116] and Lee et al. [24] investigated the effects of joining a Ti-6Al-4V coupon to a plate of the same material, as illustrated in Fig. 12. The investigations showed that the coupon penetrates the plate, generating a concave PAZ [24,116]. For a comparable amplitude, frequency and pressure the coupon to plate configuration had a 50% reduced burn-off rate when compared to a coupon to coupon weld [116]. The lower burn-off rate is likely to cause a different thermal cycle, therefore generating differing microstructures between the two welded samples even though the process input parameters were identical. However further research would be required to investigate this hypothesis. According to Astarita et al. [123], the lamella microstructure in the WCZ and TMAZ are reduced in size when higher forging forces are used to produce Ti-6Al-4V coupon to a plate welds. Unless explicitly stated, the discussions for the remainder of this article are focused on the joining of workpieces with identical contacting surface dimensions.

#### *4.1.1. Texture*

Karadge et al. [18] investigated the textures of Ti-6Al-4V laboratory (small) and full (large) scale welds. Both samples displayed a strong transverse texture $\{1\,0\,\bar{1}\,0\}\,\langle 1\,1\,\bar{2}\,0\rangle$ at the WCZ. However, the texture farther back from the weld line (TMAZ) was noticeably different between the two welds. As shown in Fig. 13, the full scale weld exhibited alternating bands of transverse $\{1\,1\,\bar{2}\,2\}\,\langle 1\,1\,\bar{2}\,3\rangle$ textures, while the laboratory scale weld did not. The precise reasons for the different textures in the TMAZ were unknown. However, it was suggested that the differences in the observed texture could be attributed to the effects of weld sizes on the temperature rise during processing and subsequent cooling. Moreover, the post-heat treatment was shown to have minimal effect on the texture results. Romero et al. [34] showed that welds produced with low pressures exhibit a strong transverse texture in the WCZ – in agreement with Karadge et al. [18] – however, welds produced with high pressures display an almost random texture at the WCZ. The reason for this observation is not entirely clear. Recent work by Guo et al. [124] showed that the texture development within a weld was highly dependent on the amount of transformed β-phase and that the deformation of the primary α-phase grains had limited effect on the texture development.

### *4.2. Mechanical properties*

Mechanical testing has shown that the hardness, using the Vickers' hardness test, in the WCZ (422 ± 11 [53], 425 ± 10 [34] and 398 ± 3 [6]) is higher than that of the parent material (302 ± 20 [53], 328 ± 20 [34] and 317–352 [6]). The increased hardness in the WCZ is due to the refined microstructure [35,42,53]. However, there appears to be some conflicting results when it comes to the hardness in the TMAZ. Some researchers suggest that the hardness in the TMAZ is between that of the WCZ and the parent material [53,58,78], as shown in Fig. 14(a), while other researchers suggest that the hardness in the TMAZ can be lower than that of the parent material [6,34], as shown in Fig. 14(b). According to Grujicic et al. [58] a coarsening of the β-grains in the TMAZ was responsible for the inferior hardness values. Romero et al. [34] stated that the conditions that cause inferior TMAZ properties are likely to be process input dependent. The researchers who achieved welds with superior TMAZ properties used higher amplitudes of oscillation. The increased amplitude may have increased the gradient of the thermal

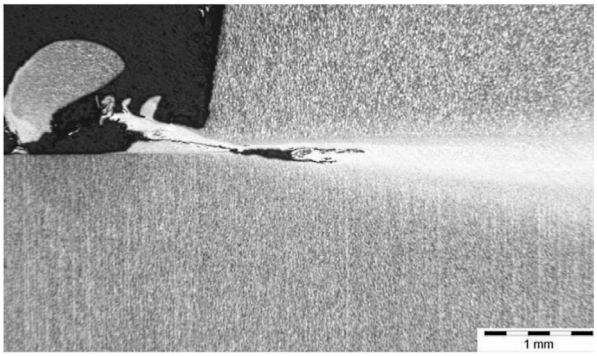


**Fig. 15.** Weld interface corner of an experimental Ti-6Al-4V 'T' joint linear friction weld showing an unbonded region (image courtesy of TWI).

profile, which in turn increased the rate of cooling once the oscillations had stopped [13]. The faster rate of cooling would have prevented grain boundary and alpha-phase lathe growth in the TMAZ [69], therefore giving superior hardness properties [69]. Kuroki et al. [78], showed that an increase of the applied pressure increases the hardness in the WCZ and TMAZ.

Assuming a Ti-6Al-4V linear friction weld is free from interface contaminants (discussed in more detail in Section 4.4), the weldment will typically fail in the parent material when tensile tested [2,6,8,22,44,78]. If interface contaminants are present the weldment will fail at the weld line. Interestingly, Wanjara and Jahazi [6] demonstrated that a weldment can fail in the TMAZ when tensile tested if it is produced with a low power input. This was possibly due to the same reason for the inferior hardness values in the TMAZ, i.e. the lower power input allowed for a shallower thermal gradient which reduced the cooling rate post-oscillatory motion [13]. This would cause increased grain boundary and alpha-phase lathe growth, resulting in the HAZ being softer than the parent material [69].

Linear friction welded Ti–6Al–4V in the as-welded state has been investigated at various stress amplitudes ranging from the high cycle fatigue (HCF) to the low cycle fatigue (LCF) regime [22,78,109,125]. According to Wen et al. [125] the fatigue cracks initiated from the surface or near-surface defects of the parent material for all cases. Stinville et al. [109] supported this observation and noticed that the crack nucleation always occurred in the parent material, regardless of the frictional pressure and maximum stress level applied. Kuroki et al. [78] showed that the HCF results were unaffected by the applied pressure used to produce the welds. Uniquely, Flipo et al. [22] showed the fatigue failure to occur along the weld region. However, it was noted that the fatigue performance exceeded the minimum design allowable values for AMS4911 [22]. The reasons for the difference between these findings are currently unclear, but it is possible the combination of process parameters used was responsible [22,109]. Recently, Flipo [126] presented the HCF and LCF results for post weld heat treated samples. The results far exceeded the values of the parent material and had minimal scatter.

The impact toughness of titanium alloy linear friction welds is much harder to predict because the microstructure is very heterogeneous [3,35,48]. However, the value at the interface of a Ti-6Al-4V linear friction weld surpasses that of the parent material [3,35].

Suleimanova et al. [127] presented the torsional strength results of linear friction welded VT6 (Russian version of Ti-6Al-4V) produced at a frequency, amplitude, pressure and burn-off of 50 Hz, 2 mm 100 MPa and 4 mm, respectively. The torsional strength value of the weld was superior to the parent material due to the test failing in the parent material at a rotation degree of 110°.

Addison [1,2] noticed that fine features of Ti-6Al-4V linear friction welds, such as the corners of the workpieces, can contain a small unbonded region; see Fig. 15. Insufficient bonding at the interface results in welds having poorer mechanical properties [2]. McAndrew et al. [117], using finite element analysis (FEA), showed that the unbonded region at the corners is very noticeable at low burn-off values. The unbonded regions can be eliminated with a burn-off increase. This is because as the burn-off increases, the heat from the flash and interface conducts into the corners causing them to soften and plastically deform. This results in the corner material merging with the rest of the interface, forming a bond at the corner and eliminating a source of inferior mechanical properties.

A repair weld involves the joining of a new workpiece onto the "stub" of a previously broken weldment. The mechanical properties and macroscopic appearance of a repaired Ti-6Al-4V weld were that same as the initial weld [1]. This is an important feature as it will allow for the repair of high-cost components, such as blisks.

### *4.3. Flash morphology*

The weld region is surrounded by the flash in all directions, as shown previously in Fig. 1(b). The mechanism in which the viscous material is forced from the weld is sensitive to the processing conditions used. For the flash generated in-plane to the oscillations, two formation mechanisms are identified for Ti-6Al-4V linear friction welds [2,7,13,14,46,108,116], one that produces "ripples" in the flash and one that produces a "smooth" morphology, as shown Fig. 16(a) and (b), respectively.

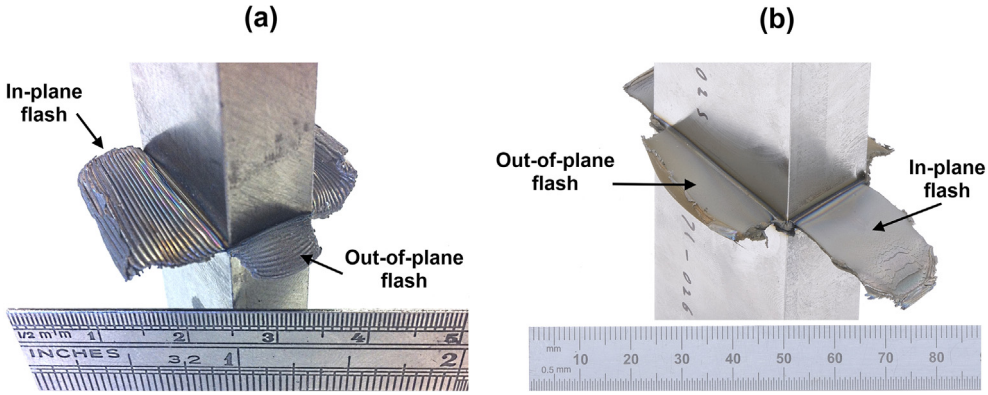


**Fig. 16.** In-plane flash observations (a) ripple morphology [13], and (b) smooth morphology [16].

The ripple morphology occurs when the flash separates from the workpieces as the maximum amplitude displacement position is approached, as shown in Fig. 17(a). At the point of separation, very high strain rates (greater than 1500 $s^{-1}$) are produced; see Fig. 17(d). The high strain rate regions correspond to significant, local yielding. This phenomenon exposes a fresh layer of highly heated material which is then sheared from the interface into the flash as the oscillatory motion is reversed. Each sheared layer corresponds to a ripple in the flash. Schröder et al. [108] and McAndrew et al. [13] demonstrated that the ripples are more noticeable when the ratio between the PAZ and the oscillation amplitude is reduced. Schröder et al. [108] suggested values below a ratio of 1 were required to generate the ripples. The "smooth" morphology is produced when the flash does not separate from the workpieces. This results in the interface material being extruded into the centre of the flash as the oscillatory motion is reversed [13,108], as shown in Fig. 17(b). Regardless of the flash morphology type, for all cases it has been shown that the boundary temperature between the rapidly flowing viscous material and the workpiece material with negligible flow approximately corresponds to the β-transus temperature for this alloy, as shown in Fig. 17(c). This is to be expected as significant material softening occurs at temperatures corresponding to the β-transus. Consequently, the thickness of the flash is directly related to the extent of material that is above the β-transus temperature, as shown in Fig. 17(c).

### 4.4. Interface contaminant removal

Interface contaminants, such as oxides and foreign particles, affect the properties [6] and possibly the service life of a weld [7] and are therefore a primary cause for a Ti-6Al-4V linear friction weld being defective [6,8,10,11,13,14]. Oxides are generated during phase 1 when the hot interface material reacts with the atmosphere [128]. It is also possible that some oxides may remain at the interface due to insufficient pre-weld cleaning. The foreign particles may constitute oil or grease from workpiece machining which were also not removed during pre-weld cleaning. At the start of phase 2 the oxides and foreign particles become trapped at the interface during the merging of the viscous material. According to Bhamji et al. [8], it is important that the contaminants are expelled from the interface into the flash as this allows for full metal to metal mixing and a bond being formed.

McAndrew et al. [13,14] and Turner et al. [7] showed that the interface contaminants are increasingly expelled into the flash as the burn-off is increased, as shown in Fig. 18. Recent research has shown that the amount of burn-off required to remove the contaminants into the flash reduces with the extent of the PAZ [13,14]. As shown earlier, the PAZ is a result of the generated band of highly heated material, consequently a smaller PAZ results in a lesser volume of rapidly flowing material being expelled with the contaminants, as illustrated in Fig. 19.

As shown in Section 4.1, the PAZ is highly dependent on the processing conditions used. Consequently, so is the amount of burn-off required to expel the contaminants from the weld interface into the flash. As shown in Fig. 20, the burn-off required to expel the contaminants from the weld interface into the flash is reduced with an increase of the pressure or a reduction of the in-plane width. An increase of the rubbing velocity minimally decreases the required burn-off. This is to be expected as the rubbing velocity minimally affects the extent of the PAZ. Based on these observations, there may be a benefit to using larger pressures and oscillating the workpieces along the shorter of the two interface-contact dimensions when producing Ti-6Al-4V welds. This is because the burn-off required to remove the interface contaminants is reduced. Hence for the same burn-off, the factor of safety on contaminant removal is greater.

Wanjara and Jahazi [6] suggested that a weld made with a low power input will have contaminants present at the interface. The low power inputs in the work by Wanjara and Jahazi [6] were produced using lower values of frequency, amplitude and pressure. The authors of this article believe that a possible reason for the existence of contaminants in the low power input welds was due to insufficient burn-off being applied for the conditions investigated [13,14].

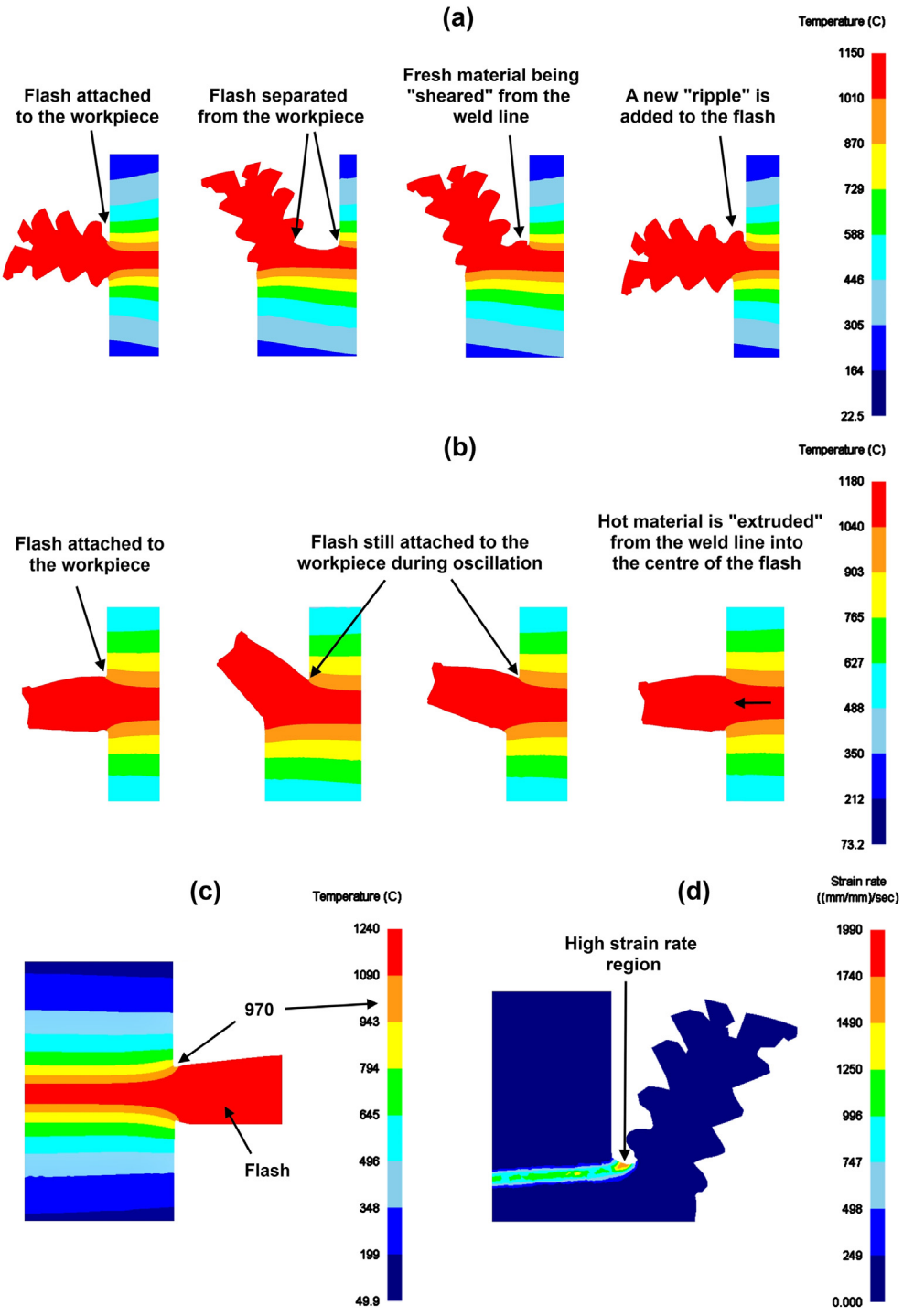


**Fig. 17.** Flash formation and morphology determined from FEA, showing: (a) the mechanisms behind the ripple morphology, (b) the mechanisms behind the smooth morphology, (c) the boundary temperature between the rapidly flowing viscous material and the workpiece material with negligible flow, and (d) region of high strain rate [13].

In rare circumstances, voids due to porosity have been observed at the interface of titanium alloy linear friction welds [6,39,44]. This often occurs when comparatively low values of burn-off are used. Lang et al. [39] noticed that the voids are typically located toward the edges of the weld interface for titanium alloy welds. This suggests that the porosity was due to an initial foreign particle (probably trapped surface gasses) which had not been expelled into the flash due to an inadequate amount of burn-off. This is believed because defects typically associated with fusion welding processes, such as

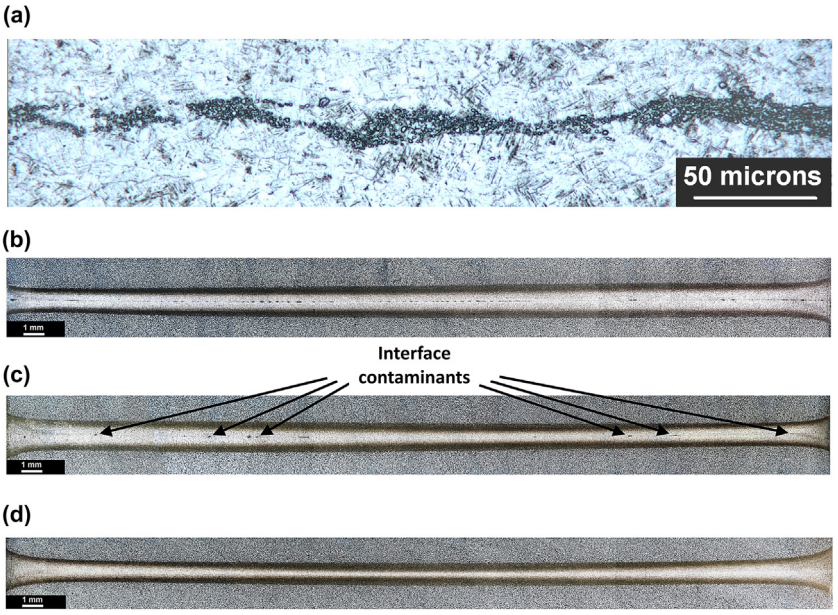


**Fig. 18.** (a) High magnification of the contaminants present at the weld interface of a Ti-6Al-4V weld, (b) contaminants after 0.5 mm of burn-off, (c) contaminants being expelled toward the edges after 1 mm of burn-off, and (d) no contaminants after 3 mm of burn-off [14].

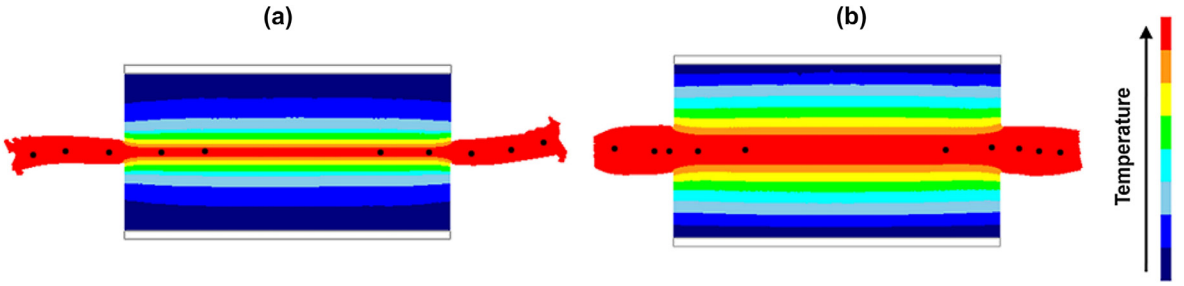


**Fig. 19.** An illustration of the contaminants (black dots) entrapped in a band of rapidly flowing material (red contour) for: (a) a thin band of rapidly flowing material, and (b) a large band of rapidly flowing material.

porosity, are typically avoided during solid-state joining process. This is primarily due to the avoidance of the melting and solidifying of the material [11,42,51–57].

### *4.5. Residual stresses*

Residual stresses are present in Ti-6Al-4V linear friction welds after processing [34,47,70]. The residual stresses are generated via two mechanisms. The first is due to the plastic deformation experienced by the workpieces at elevated temperatures [51,107]. The second is due to the thermally induced strain [47,129], which results from the difference in thermal expansion and contraction of the material during heating and cooling. The primary mechanism is due to the thermally induced strain that occurs during the post-oscillatory motion cooling [47]. Understanding residual stress formation is important because it negatively influences weld performance and life [8,47,107].

Residual stresses have been investigated for Ti-6Al-4V linear friction welds using:

- Non-destructive testing, such as synchrotron X-ray diffraction [34,47,70] and neutron diffraction [107]. Both of these methods involve calculating the strains and stresses from changes in the crystal lattice spacing.
- Destructive testing, such as the contour method [70,107]. The contour method is far cheaper than the non-destructive methods, but the residual stresses are only measured in the plane of the sectioning, i.e. the contour. With respect to LFW, the contour method tends to show good residual stress profile correlation with well-established measuring techniques (i.e. non-destructive), however the peak tensile stresses tend to be underestimated [70,107], even by as much as 200 MPa [70].

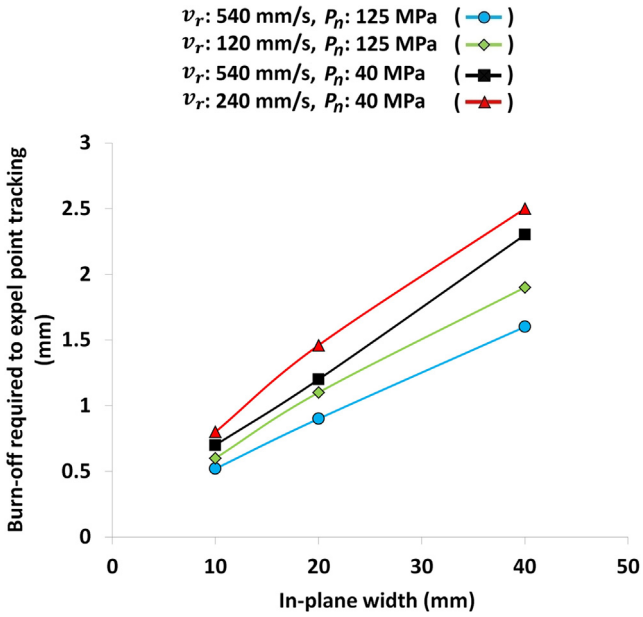


**Fig. 20.** The amount of burn-off required to expel the interface contaminants (denoted as point tracking in FEA) as a function of the in-plane width, rubbing velocity, $v_r$, and pressure, $p_n$ [13].

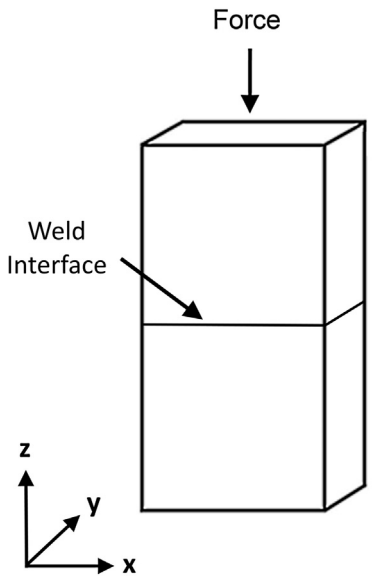


**Fig. 21.** Residual stress formation with respect to the workpiece dimensions. Note that 'x' is larger than 'y'.

- Numerical models [47,130–132]. Provided suitable input data is used, models have been able to predict the origin of residual stresses.

Regardless of the process input combination and direction of oscillatory motion used, there is a broad agreement [34,47,70,107,131,132] that the residual stresses are generally largest in the direction of the longest contacting surface dimension ('x' in Fig. 21). Followed by the shortest contacting surface dimension ('y' in Fig. 21), and lowest in the direction normal to the weld plane ('z' in Fig. 21). The residual stresses at the weld interface tend to be tensile with peak values of around 600–1000 MPa being common [34,47,107]. As shown in Fig. 22, a sharp drop in the stresses either side of the weld line is often observed, becoming compressive until they eventually approach zero [34,47,70]. Romero et al. [34] and Bhamji et al. [8] claimed that since the weld plane is longer in the 'x' direction than in the 'y' direction it is likely that there is a larger

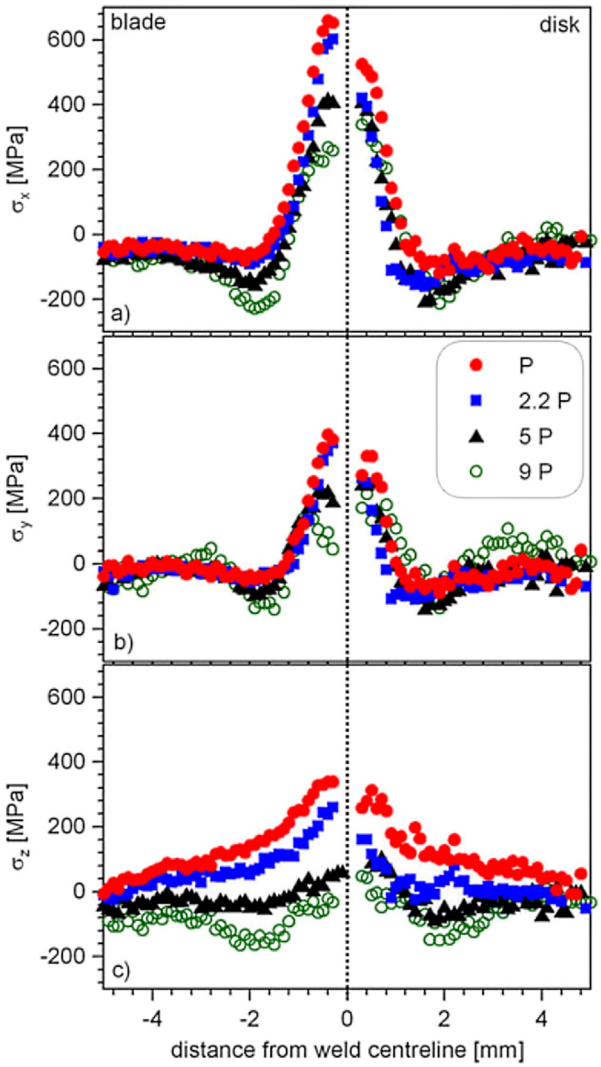


**Fig. 22.** Influence of the forging pressure 'P' on the residual stress components in the x, y, z coordinates [34].

thermal gradient in the 'x' direction, hence the increased residual stress. Bhamji et al. [8] also claimed that the small thermal mismatches in the 'z' direction may be related to the high weld pressure that is applied in the axial direction, which results in sufficient plasticity to compensate for any mismatch. The authors of this article, however, believe that another reason for the lower residual stress values in the 'z' direction is due to a uniform expansion and contraction of hot material which therefore generates a plastic strain field with very few mismatches along this direction.

Post-weld heat treatment (PWHT) has been shown to significantly reduce the residual stresses in linear friction welds [70], even by as much as 90% [8]. According to a review by Bhamji et al. [8] the residual stress relief is dependent on the size of the workpiece geometry. For example, in a comparatively smaller welded sample negligible residual stress remained after PWHT, whereas in a larger welded sample significant stresses remained after an identical PWHT. Both welds displayed similar residual stress profiles prior to PWHT. In addition to residual stress relief, PWHT is also used to homogenize the microstructure [89] and improve the mechanical properties [44] of linear friction welds.

Romero et al. [34], Nikiforov et al. [130], Fu et al. [132] and Turner et al. [47] showed that the peak tensile residual stresses can be minimised if a weld is produced with higher applied pressures, as shown in Fig. 22. As detailed in Section 4.1, this phenomenon can be explained by the relationship between the pressure and interface temperature. The higher pressures reduce the interface temperature and therefore the thermal mismatch, which reduces the residual stress intensity [34]. Recent FEA work by Bühr et al. [131] demonstrated that a high rubbing velocity produced a higher peak tensile residual stress at the weld interface ('x' and 'y' in Fig. 21) distributed over a narrow region, while a lower rubbing velocity produced a lower peak residual stress distributed over a wider region. Interestingly, in the applied force direction ('z' in Fig. 21) the trends of the rubbing velocities on the peak tensile stress values were reversed.

### 4.6. Energy usage

Several authors [3,6,31,32,48,53] have investigated the effects of the process inputs on the power density input for Ti-6Al-4V linear friction welds using Eq. (2) or Eq. (3):

$$q' = \mu \cdot P_n \cdot v_r \tag{2}$$

where $q'$ is the power density, $v_r$ is rubbing velocity, $P_n$ is normal pressure, and $\mu$ is coefficient of friction.

$$q' = \frac{A \cdot f \cdot P_n}{2 \cdot \pi \cdot A_s} \tag{3}$$

where $q'$ is the power density, $A$ is the amplitude of oscillation, $f$ is the frequency of oscillation, $P_n$ is the normal pressure and $A_s$ is the cross sectional surface area.

Analysis of the units in Eq. (3) indicates that the parameters on the right do not give the correct units for power per unit area. This may be due to a poorly named variable; the pressure term should have been force. Also, the coefficient of friction is not considered. Regardless of the equation used, many of these authors used average values for the rubbing velocity, coefficient of friction and pressure, thus only giving an approximation of the power input. In addition, they did not investigate the effects of the process inputs on the overall energy required to make a weld, which is of economic and environmental concern [49].

Ofem et al. [49], addressed this by demonstrating that the output data from a LFW machine can be used to calculate the instantaneous power input, $q$ in the form of [49]:

$$q = F_{int} \cdot v \tag{4}$$

where $F_{int}$ is the interface force of the workpieces and $v$ is the instantaneous velocity. By integrating equation 4 as a function of time, the overall energy used to make a linear friction weld can be estimated:

$$E_x = \int_0^{t_t} F_{int} \cdot v dt \tag{5}$$

where $E_x$ is the total energy inputted to a weld; and $t_t$ is the total time to make the weld.

This method of calculating the power and energy includes the effects of the changing velocity and friction coefficient over each cycle of oscillation. McAndrew et al. [15] expanded on the approach identified by Ofem et al. [49] to investigate the energy usage of Ti-6Al-4V linear friction welds. It was shown that there is an advantage to using high rubbing velocities to minimise the overall energy input required to make a weld. This was a consequence of the higher power input generated by the larger rubbing velocities, which caused the interface material to heat and plasticise more rapidly during phase 1, then shorten much more rapidly during phases 2 and 3. This reduced the overall duration of the weld and hence the energy wasted due to conduction, convection and radiation. An increase of the applied pressure had a similar effect on the energy required to make a weld for the same reasons as the rubbing velocity. An increase of the burn-off was shown to increase the overall energy required to make a weld due to the longer duration of the process. Moreover, analysis of LFW machine data indicates that the rubbing velocity has a far greater effect on the generated power input than the applied pressure [15,74,133].

### 4.7. Tooling effects

There have been relatively few investigations into the effects of the LFW machine tooling (workpiece clamping) on the processing of linear friction welds. The authors are only aware of two such investigations [122,134].

Li et al. [122] analysed high-speed photography of the LFW process and noticed that the workpieces do not oscillate in a rigid manner. In fact, it was noticed that the workpieces can move in the clamps, which generates a "micro swing" effect; see Fig. 23. A model was produced to investigate this effect for Ti-6Al-4V welds. The models showed that the burn-off rate increased with larger angles of micro-swing, which was due to one workpiece digging further into the other and extruding more material per cycle. According to Li et al. [122], the different micro-swinging angles had negligible effect on the interface temperature at the centre of the weld.

Yamileva et al. [134] investigated the effects of the clamping distance from the weld interface (denoted by 'H' in Fig. 24(a)) on the phase 1 thermal profiles in Ti-6Al-4V welds. The 'H' value was shown to have a significant effect; see Fig. 24(b). It is unclear at what point during phase 1 the thermal profiles were recorded, although it is very unlikely that it was at the end of the phase as the β-transus temperature had not been reached [15]. Unfortunately the work did not investigate the effects of the clamping during the flash forming phases of the process. This would have been an interesting investigation as the clamping may have an impact on the interface contaminant expulsion if the generated thermal profiles are widely different [13,14].

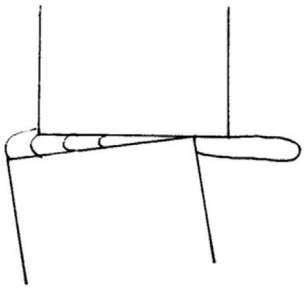

**Fig. 23.** An illustration of the "micro-swing" effect for Ti-6Al-4V linear friction welds [122].

## 5. Process modelling

In practice, many aspects of the LFW process are difficult to measure experimentally, particularly the phenomena associated with the weld interface, such as the temperature and deformation history. This is primarily due to the rapid nature of the process and the fact that the interface of the workpieces cannot be observed during welding. Computational modelling offers a pragmatic way to investigate the weld cycle history, allowing for an insight into the rapidly evolving process [7,47,48,135]. Weld modelling may be divided into two categories: analytical and numerical.

### 5.1. Analytical modelling

Analytical models use equations to predict the outputs from the process [136]. The models often involve many simplifications, such as constant material properties [7,32,46] and one-dimensional heat flow [32], however a good match with experimental results can still be attained [7,32,46,136]. From a practical point of view, analytical modelling of heat flow has the advantage of being easier to setup [137] and can have quicker computational times than numerical models [136].

There are a limited number of papers published on analytical modelling of the friction welding processes and even fewer on linear friction welding [7,32,46,138–140]. This is due to the complexity of these thermomechanical processes and the small number of active research groups on linear friction welding worldwide. These limitations are affecting all friction welding variants but are pronounced in the case of LFW, which has the additional disadvantage that researchers who engage in research in the most studied variant of FSW do not apply their expertise to LFW. As stated, the literature on analytical models of Ti-6Al-4V linear friction welding is relatively sparse when compared to experimental and numerical investigations. Some of the primary findings are reported below.

#### 5.1.1. Phase 1 thermal modelling

Vairis and Frost [32] developed thermal model for the LFW of Ti-6Al-4V workpieces during phase 1. The one-dimensional thermal model was based on the "*heat flux being applied to a solid bounded by two parallel planes*" approach, described by

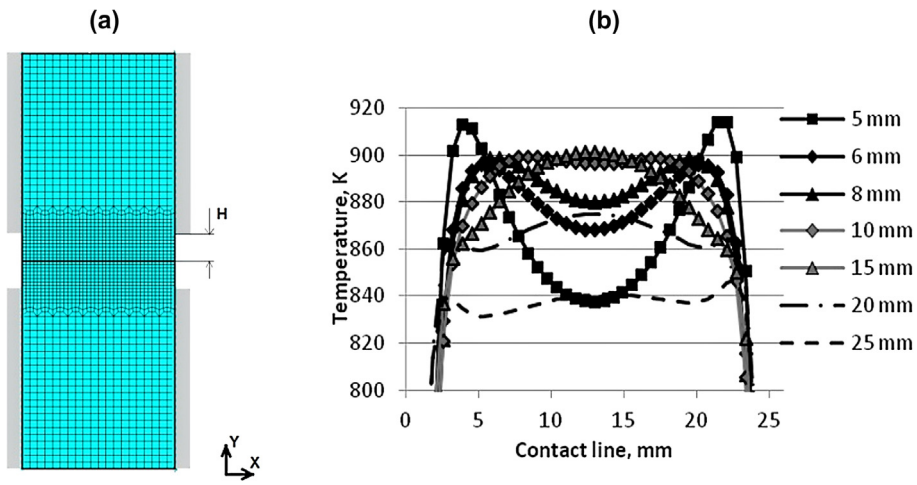


**Fig. 24.** Clamping effects: (a) a model showing the parameter 'H' that was varied, and (b) the generated phase 1 thermal profiles with different values of 'H' for Ti-6Al-4V linear friction welds [134].

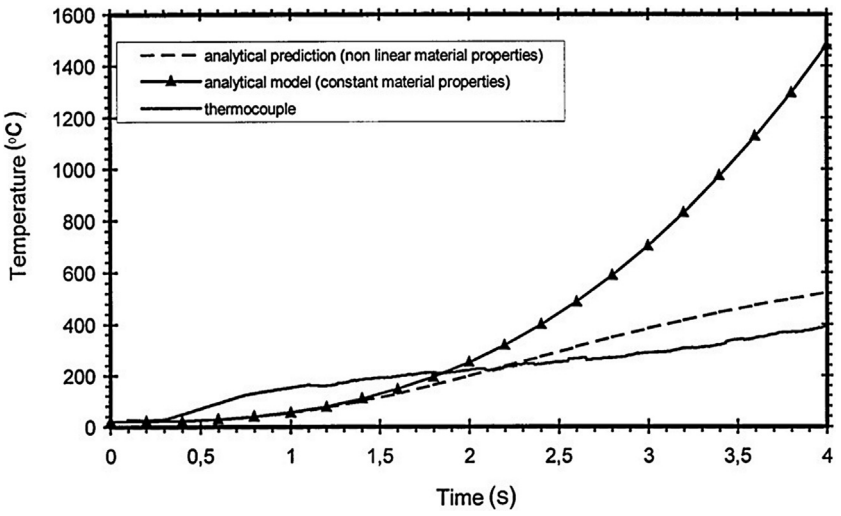


**Fig. 25.** Comparison between the analytical models and experimental thermocouple data at 1.6 mm back from the interface during phase 1 [32].

Carslaw and Jaeger [141]. One of the parallel planes was assumed to be the rubbing surface. This allowed for the temperature, T, at any distance back from the interface, x, as a function of time, t, to be determined. The equation was as follows:

$$T = \frac{2^{(m+1)} q_0 k^{\frac{1}{2}} t^{\frac{(m+1)}{2}} \Gamma\left(\frac{1}{2}m+1\right)}{k} \sum_{n=0}^{\infty} \left\{ i^{m+1} erfc \frac{(2n+1)L_0 - x}{2(kt)^{\frac{1}{2}}} + i^{m+1} erfc \frac{(2n+1)L_0 + x}{2(kt)^{\frac{1}{2}}} \right\} \tag{6}$$

where $k$ is the diffusivity, $\Gamma$ the Euler gamma function, $L_0$ is the length of overhang of the workpiece, $m$ is a constant, $q_0$ is the heat flux, $I$ is the temperature from the previous iteration, and the term $erfc\{x\}$ is the complementary error function.

Vairis and Frost [32] assumed the following for their model:

- the heat flow was one dimensional
- there was no heat loss to the surrounding environment
- the co-efficient of friction linearly increased with the time from 0.25 to 0.55
- the true area of contact increased linearly with time from 0% to 100%
- the model was static, i.e. there was no transverse movement of the workpieces

As seen in the assumptions, the work by Vairis and Frost [32] assumed no movement of the workpieces, so the model does not account for the reciprocal movement with variable velocity. The model was investigated with linear (constant) and non-linear (change with temperature) material properties. The results were compared to thermocouple recordings. As can be seen in Fig. 25, the modelled temperature rise deviates significantly from the experiment values after two seconds for the conditions that used constant material properties. The model that used non-linear material properties provided a better prediction of the experimental temperature. Vairis and Frost [32] noted that the contribution of the exothermic reaction between Ti and oxygen during phase 1 of the LFW process was shown to be negligible, despite the impressive visual effects added to the welding of Ti-6Al-4V.

Although suitable for modelling the thermal fields during phase 1 of the LFW process, questions of the applicability of the model must be raised for modelling the phase 3 thermal profiles; the model does not account for the burn-off, which helps to cool the weld interface. The burn-off during phase 3 allows for a steady-state condition to be achieved, i.e. the heat expelled during the burn-off approximately equals the heat generated from the viscous plastic deformation. Consequently, without the inclusion of the burn-off, the temperature throughout the analytically modelled workpieces keeps rising and never reaches a steady-state condition.

*5.1.2. Phase 3 (Steady-State) thermal modelling*

Turner et al. [7] proposed a one-dimensional heat flow model for estimating the thermal profiles during phase 3 of the LFW process:

$$T = T_0 + [T_{flash} - T_0] \cdot \exp\left\{ -\frac{v_{ss} \cdot \mathrm{x}}{\alpha} \right\} \tag{7}$$

where $T$ is the temperature at any point, $x$, back from the interface; $T_0$, is the initial temperature of the material; $T_{flash}$ is the temperature of the flash/interface region; $v_{ss}$ is the steady-state burn-off rate; and $\alpha$ is the thermal diffusivity (which was

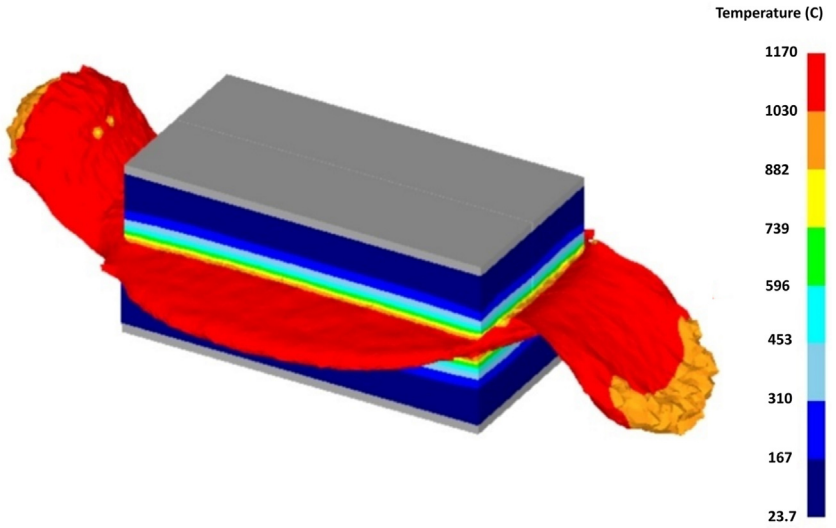


**Fig. 26.** A three dimensional Ti-6Al-4V LFW process model [117].

assumed to be temperature independent). Prior knowledge of the steady-state burn-off rate, $v_{ss}$, and the interface temperature, $T_{flash}$, are required for the analysis, meaning the model has to be used retrospectively.

Turner et al. [7] compared the thermal profiles generated from their analytical model to those from numerical models. In general, good comparisons were made for Ti-6Al-4V welds.

Schroeder et al. [46] manipulated equation 7 to estimate the thickness of the heat affected zone during phase 3 of the process for Ti-6Al-4V workpieces. The equation was as follows:

$$x_{HAZ} = \alpha \cdot log[(T_{flash} - T_0)/(T_{HAZ} - T_0)] \cdot A_s \cdot \rho \cdot H \cdot (T_{flash}) \cdot q^{-1} \quad (8)$$

where $x_{HAZ}$ is the thickness of the HAZ, $\alpha$ is the diffusivity, $T_{flash}$ is the temperature of the flash, $T_0$ is initial temperature of the material, $T_{HAZ}$ is the temperature of the HAZ furthest away from the interface (assumed to be 900 $^{\circ}$C), $A_s$ is the area of the mating surfaces, $\rho$ is the density, $H$ is the specific enthalpy, and $q$ is the power input. With the exception of the power input, all of the parameters were assumed to be constant. In general, the model predicted the experimental trends well [46].

### 5.1.3. Phase 3 (Steady-State) strain rate modelling

Vairis and Frost [31], adapted a rotary friction welding analytical model to predict strain rates at the interface of Ti-6Al-4V linear friction welds. The semi-empirical model was able to estimate interface strain rates for the different Cartesian directions of the weld interface ('y' and 'x' in Fig. 1(b)). It was shown that the strain rates were highest at the weld interface and decreased farther back. The model showed that the strain rates appeared to be largest in the direction out-of-plane to oscillation, i.e. the 'y' direction in Fig. 1(b). Moreover, the strain rates were shown to increase with an increase of the frequency of oscillation, however, the peak values recorded from the analytical model (3.5 $s^{-1}$) were much lower than those recorded by the numerical models of Turner et al. [7] (2500 $s^{-1}$) and McAndrew et al. [13,14] (860–1740 $s^{-1}$).

## 5.2. Numerical modelling

Analytical models often employ many simplifications, such as constant material properties [7,32,46] and one-dimensional heat flow [32]. This limits their ability to provide accurate information in complex process situations [10,142]. Therefore, for welding simulations, computational numerical modelling is often employed to discretise a problem into more manageable sub-problems. The solutions to these problems are then approximated at finite time steps [136,143,144].

To the authors' best knowledge, all computational numerical investigations into the LFW process for the joining of Ti-6Al-4V used finite element analysis (FEA) [7,13–16,24,32,46–48,58,108,116,121,122,130,134,144–152], which is also referred to as the finite element method/modelling (FEM). Several FEA packages have been used to model the LFW process, including: Abaqus, Ansys, DEFORM, Elfen and Forge. Fig. 26 shows an example of a numerical LFW process model developed using DEFORM.

LFW process models have been used to obtain data on various Ti-6Al-4V weld responses, such as: residual stress formation [47], interface contaminant expulsion [7,13,14,24], strain rates [7,13,14], flash morphology [7,13,14,46,108,116], flash formation rates [7,13,14,46,48] and thermal fields [7,13–15,24,32,46–48,58,116,150,153,154]. The primary advantage of FEA is that it allows for the prediction of many outputs that are difficult to obtain experimentally.

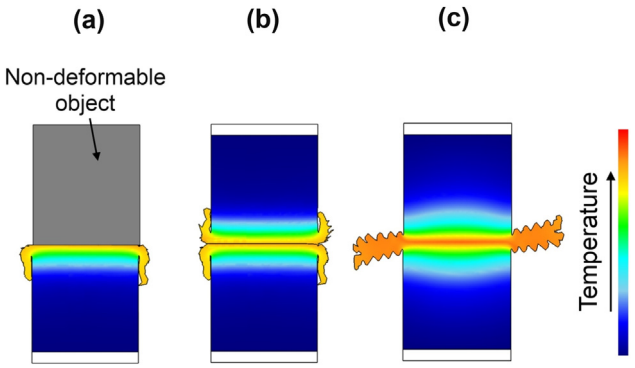


**Fig. 27.** Modelling approaches: (a) one workpiece, (b) two workpieces (c) a single body representing two workpieces [13,14].

*5.2.1. Reference frames and meshing*

The meshing of a model should be tailored to the outputs of interest. For example, a model that is required to predict plastic deformation will require a finer mesh than a purely thermal analysis [144]. A decrease of the average mesh element size increases the accuracy of the results but results in more elements being required, increasing the computational time [7].

As the plastic deformation primarily occurs at the interface during LFW, many authors use a mesh that is finer at the interface and coarser farther back. Typical interface mesh element lengths used for LFW process models are between 1 mm and 0.08 mm [7,13–16,24,32,46–48,58,108,116,121,122,130,134,144–152]. 2D modelling values tend to be closer to the latter end of the scale, with values below 0.25 mm being optimal for capturing the flash morphology [7,13,14,46,144]. 3D LFW process models require substantially more time than 2D models to complete a simulation due to the increased element count, and terms included in the heat and mass flow equations. Consequently, authors often trade some of the accuracy of the results to decrease the simulation time. This is achieved by using larger elements at the interface region (0.5–1 mm) [16,117,122,149]. This approach is also used in other 3D friction based process models. For example, when using DEFORM to 3D model the friction stir [155–157] and friction stir spot [158] welding processes the plastic deformation zone was meshed with elements of between 0.8 mm and 0.5 mm in length – values considerably larger than 0.25 mm.

The "Arbitrary Lagrangian Eulerian" (ALE) approach was developed for solving problems that could not be suitably described by the Eulerian or Lagrangian approach [136]. The ALE approach, as the name suggests, is a hybrid of the Eulerian and lagrangian methods. The ALE approach allows a mesh to function in the traditional Lagrangian fashion until the mesh becomes too highly distorted. During a re-mesh the most distorted regions of the mesh are then repositioned to a predefined Eulerian mesh density. The ALE approach appears to be the dominant method used when producing FEA process models of Ti-6Al-4V linear friction welds [13–15,46,48,58,98,108,116,149,153].

*5.2.2. LFW modelling approaches*

Various authors have developed two and three dimensional (2D/3D) computational Ti-6Al-4V LFW process models [7,13–15,24,46–48,58,108,113,116,121,134,145,147,149,151,152,159]. The majority of the modelling work consists of 2D models, which have been shown to successfully provide an adequate insight into many of the phenomena associated with LFW, as previously shown in Fig. 17. As stated above, the main advantage of 2D models is the quicker simulation times. This makes 2D models particularly suitable for parametric studies [16,117]. However, by their nature, these models are unable to replicate the flash transverse to the direction of oscillation, therefore limiting full process behaviour understanding [14]. 3D models have the advantage of providing an insight into the full multi-directional flow behaviour. This is particularly useful to understand the material flow and thermal cycles at the corners of the workpieces – something 2D models cannot do.

According to the literature, there are three "traditional" approaches that can be used to model the LFW process. The first approach, as evidenced by the early work by Vairis and Frost [32] involved modelling only one workpiece, which was oscillated against a non-deformable surface, as illustrated in Fig. 27(a). This approach allows for quicker computational times as only half of the geometry is modelled. The problem, however, is that the coefficients of friction need to be known so that the thermal aspects of the model during phase 1 can be predicted accurately. Furthermore, due to only one workpiece being modelled, it is impossible to model the flow behaviour after the two workpieces merge to each other; see Fig. 3(b).

As computational power increased, many authors expanded on the early approach to develop the second modelling approach, which considered both workpieces [48,58,121,134,145,147,149,151,152], as illustrated in Fig. 27(b). Many of the problems with this approach are the same as the first. For example, despite considering both workpieces, models of this type show that they never truly merge during phases 2 and 3 – as happens in reality for Ti-6Al-4V [2,6,13,15] – meaning the flow behaviour after the workpieces merge is still not considered.

The third approach, as shown in Fig. 27(c), was developed by Turner et al. [7], who noticed that prior to the workpieces merging there is negligible macroscopic plastic deformation, at least for the titanium alloy Ti-6Al-4V. Once a

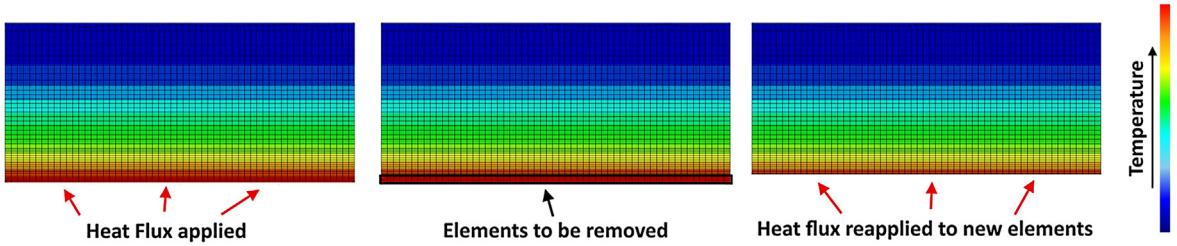


**Fig. 28.** A schematic of the step-wise modelling approach developed by Bühr et al. [131].

viscous layer is formed the process may be modelled as a single-body due to there being full contact between the two workpieces. A temperature profile needs to be mapped onto the single-body model to account for the heat generated prior to merging. This is vital, as the temperature profile will result in a low flow-strength for the material at the centre. This enables the material at the centre to deform in preference to the surrounding material, allowing the single body to represent two individual workpieces. Due to the merging of the interface material being modelled, this approach considers the true interface flow behaviour and produces much better replications of the flash morphology for Ti-6Al-4V workpieces [7,13,14,46,108]. The limitation of this approach is that the stages prior to workpiece merging are not modelled.

In addition to the geometry setup, the user has the ability to decide on the type of analysis the model will provide: purely thermal, elastic-plastic or plastic. The thermal analysis neglects the elastic and plastic effects, and requires very little computational time. The elastic-plastic analysis allows for the inclusion of the elastic and plastic effects, therefore providing greater accuracy and insight, however considerable computational time is added. Purely plastic models neglect the elastic effects and assume incompressible flow, which is generally considered to be a "reasonable" assumption when significant plastic deformation occurs [136]. Consequently, plastic models require less computational time than the elastic-plastic analysis. Turner et al. [7,47], Schroeder et al. [46,108,116] and McAndrew et al. [13,14] demonstrated that a purely plastic analysis during the oscillatory phases of the LFW process is sufficient to accurately capture the experimental trends. However, the elastic-plastic analysis must be used during the post-oscillatory motion cool down period if the residual stress formation is to be modelled [47].

Turner et al. [47] highlighted that the stresses generated during the oscillatory phases of the process (i.e. phases 1–3) only play a minor role on the final residual stress field. This is because the temperatures recorded during phase 3 are above the beta-transus temperature [13,14,60], allowing the material to reach a viscous state. Therefore, the stresses generated at these temperatures are comparably very low [7,14,15,116] and are unlikely to affect the overall final residual stress field. The residual stresses are primarily driven by the final thermal distribution and are principally generated during the post-oscillatory motion cooling period [47]. Consequently, Bühr et al. [131,160] hypothesised that it is unnecessary to use the three "traditional" LFW modelling approaches if only the residual stress field is of concern, as modelling of the oscillatory motion is time consuming [16], involving complex re-meshing techniques. Bühr et al. [131,160] proposed a novel LFW modelling approach that bypasses the dynamic oscillatory phases of the process and focuses on the post-weld cooling period, i.e. the modelling approach targets the residual stress formation. To account for the thermal fields generated during processing, Bühr et al. [131,160] applied a heat flux to the interface of their model. To account for the burn-off, a row of elements were removed from the interface in a step-wise manner. The heat flux was then reapplied to the new elements. A schematic of the modelling approach is shown in Fig. 28. Once the desired burn-off had been modelled the model was allowed to cool down to predict the residual stress fields. The modelled thermal histories matched experimental thermocouple recordings well, suggesting the simplified modelling approach is indeed viable as a numerical tool. However, experimental validation of the model's residual stress fields had not yet occurred.

### *5.2.3. Coupled analysis and process efficiency*

All welding simulations generally comprise a thermal analysis and a mechanical analysis. These can be run simultaneously (coupled) or independently (decoupled). A decoupled analysis works on the principle that the thermal analysis is run first and is used to form the basis of the subsequent mechanical analysis, i.e. no heat is generated during the mechanical analysis. The analysis must be coupled if the mechanical aspects are going to have an impact on the thermal fields. Due to a substantial amount of heat being generated via plastic deformation of the interface material during LFW, LFW process models must use the coupled analysis if the oscillatory phases are to be dynamically modelled [144].

During friction welding simulations the amount of mechanical energy estimated to be converted to heat when plastically deforming the material varies. Typical values used are 90% [13,14,24,48,55,142,155] and 95% [58,96,108,158]. The remainder of the energy is assumed to be associated with the phase transformations, changes in the grain boundary generation and migration, dislocation density and evolution, and stored in the form of crystalline defects [96,155]. Some authors, however, have assumed an efficiency of 100% [7].

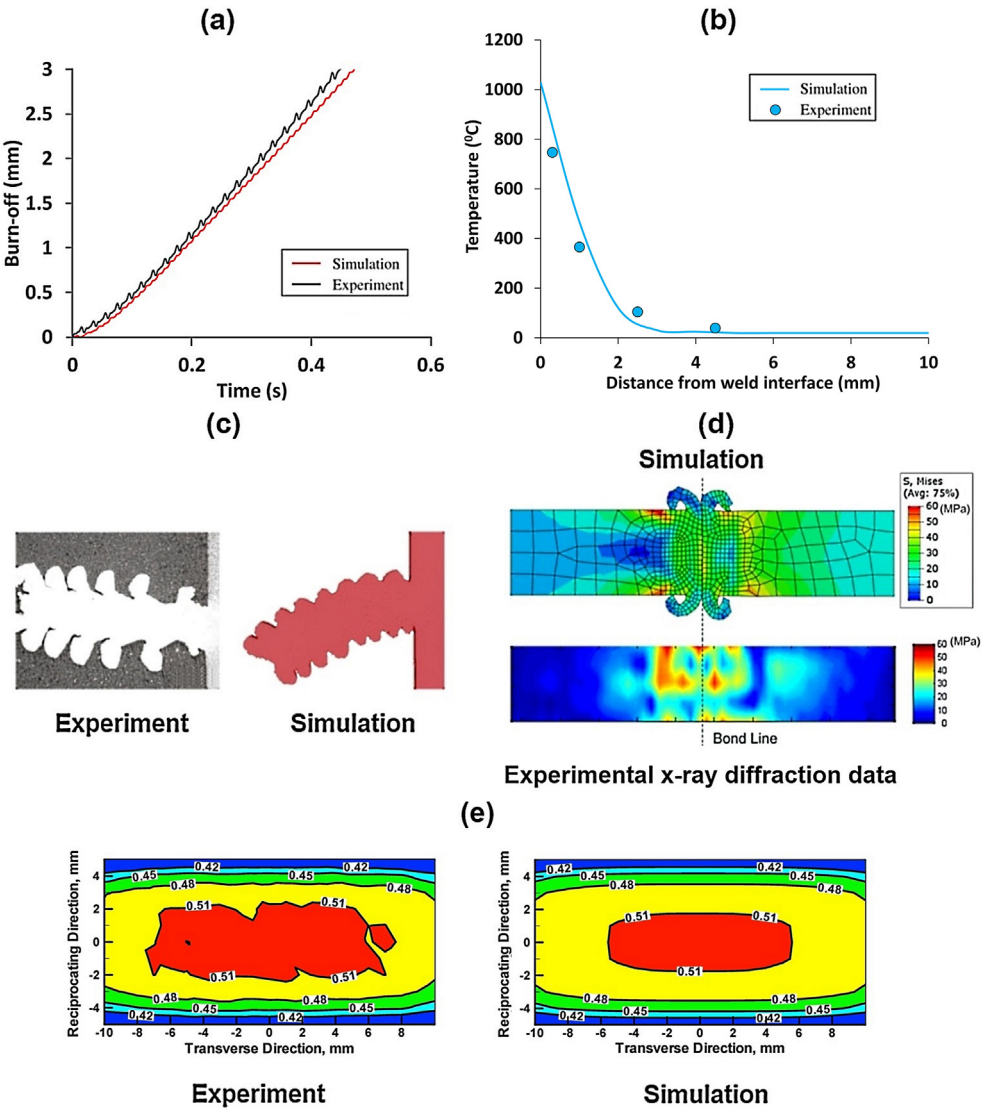


**Fig. 29.** Modelling validation displaying: (a) burn-off histories for Ti-6Al-4V workpieces [13]; (b) thermal profile at the end of phase 1 for a Ti-6Al-4V weld [15]; (c) flash morphology for a Ti-6Al-4V weld [7]; (d) residual stresses in an aluminium alloy weld [93]; and (e) the spatial distribution of the precipitate mean radius (in microns) over the mid-plane/contact surface of the LFW joint in a Carpenter Custom 465, H1000 [96].

*5.2.4. Constitutive data*

Two different approaches have been used to account for the material constitutive data in LFW process models for the joining of Ti-6Al-4V. This includes using a tabular format [7,13,14,24,32,47,55] (showing flow stress values at different strains, strain rates and temperatures) or equation based models [7,48,58,153], such as the Johnson-Cook model. According to Turner et al. [144], each approach has its own advantages. For example, the tabular approach generally appears to be much more robust and reliable - assuming the FEA code does not have to extrapolate too much outside the region where the data is available. However, this approach is less computationally efficient. In the authors' opinion, extra care should be taken when using equation based models as they do not always accurately represent the true flow stress behaviour over the regime of interest [16]. In addition, some of the models exclude or give poor representation of the fundamental behaviour. For example, the Johnson-Cook model gives poor flow stress estimates at low strain rates and the flow strength linearly reduces to zero with temperature, which rarely occurs in practice; and the Zener-Hollomon model excludes the strain effects [136].

*5.2.5. Validation*

A model's accuracy is highly dependent on the material properties, boundary conditions and assumptions used. The most important fact to remember is that a model is just an approximation of a real-life engineering problem. Agreeing with Reilly [136] and Turner et al. [7], models must be critically compared to experiments to test their validity. Successful validation for

a range of outputs allows for the data predicted by the models that are non-amenable to experimental measurement to be trusted. In addition, without validation the results may be unreliable to form a basis for further investigation. To date, the following experimental responses – for a range of materials not just Ti-6Al-4V – have been used to validate LFW process models: burn-off histories [7,13,14,46,52,55,76,93,95,153,161], flash morphologies [7,13,46], thermal histories [7,14,15,32,46,153,162], residual stresses [47,93], shear forces [13,14,32], and the average microstructural grain radius and spatial distribution [96], as shown Fig. 29. Fig. 29 also shows that LFW process models frequently capture experimental trends, confirming that modelling does provide an insight into the process.

## 6. Conclusions

This section presents a summary of the article findings, practical implications of the findings and recommendations for further research. This section should allow the reader to appreciate the benefits and have a better understanding of the LFW process for the joining Ti-6Al-4V, hopefully allowing for further process development and exploitation.

### *6.1. Summary*

A review of the published literature on the linear friction welding of Ti-6Al-4V was conducted. The key findings from the review are summarised below:

- Linear friction welding utilise the heat generated during friction to produce solid-state bonds. When compared to other friction welding processes, where there are numerous publications, relatively little investigation has taken place into the LFW process. Although, there have been an increasing amount of LFW publications in the last five years.
- The LFW process works by oscillating one workpiece relative to another while under a large, compressive force. Although one continuous process, LFW occurs over four phases: initial, transition, equilibrium, and deceleration and forging. The process is controlled by eight inputs, but the oscillation amplitude, oscillation frequency, applied force (pressure) and burn-off are believed to be the most influential.
- LFW is an established technology for the manufacture of titanium alloy integrated bladed disks (blisks) for aero-engines. However, due to the many benefits the process offers it is finding increasing interest for the manufacture of aircraft structural components – particularly for Ti-6Al-4V.
- Components machined from a solid block (ingots, forgings and extrusions) are expensive due to the proportionally large amount of material that is purchased compared to the amount that remains after machining. LFW reduces the material required to make a component by joining smaller workpieces to produce a preform, which is subsequently machined to the desired dimensions. This brings substantial improvements to the buy-to-fly ratios, which significantly reduces manufacturing costs. The linear friction welded components also have a comparable strength and quality to machined parts.
- In addition to the economic benefits, LFW offers many advantages over traditional fusion welding methods, including: excellent mechanical properties; avoidance of melting, allowing for a range of dissimilar materials to be joined; and very low defect rates.
- LFW machines are capable of delivering the dimensional precision, with high repeatability, required by the aerospace industry.
- Much of the academic research into the LFW process is for welds with a single-surface of contact. There is an interest from industry to investigate the LFW process for non-planar surfaces, such as the "keystone" geometry.
- Ti-6Al-4V linear friction welds are similar in appearance in that they have several distinct zones: a weld centre zone (WCZ), a thermo-mechanically affected zone (TMAZ) and a heat affected zone (HAZ), and are surrounded by the expelled interface material (flash). The extent and microstructural composition of these zones are highly dependent on the processing conditions used.
- The thermal profiles generated in the welds are very dependent on the processing conditions used. In general, an increase of the rubbing velocity (amplitude and/or frequency) increases the interface temperature while reducing the extent of the HAZ. An increase of the applied pressure decreases the extent of the HAZ and the interface temperature. A decrease of the in-plane width also reduces the extent of the HAZ and the interface temperature.
- The WCZ consists of a strong transverse texture regardless of the weld size. However, the TMAZ in larger welds exhibit an alternating bands of transverse $\{1\ 1\ \bar{2}\ 2\}\ \langle 1\ 1\ \bar{2}\ 3\rangle$ textures, while small size welds do not. The WCZ texture appears to be stronger with lower pressures. Moreover, the weld textures are minimally affected by PWHT.
- The tensile, microhardness, torsion and impact properties of Ti-6Al-4V welds tend to be superior in the WCZ due to the refined microstructure. In general, the fatigue performance (as-welded and PWHT) of the WCZ also appears to be superior, although there is published literature to the contrary.
- The flash morphology of a Ti-6Al-4V linear friction weld is dependent on the processing conditions used. The ripple morphology is more noticeable when the ratio between the PAZ and the oscillation amplitude is below 1.

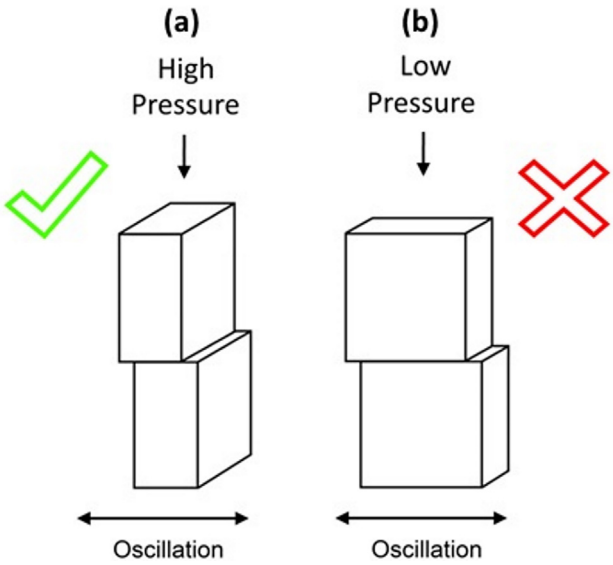


**Fig. 30.** An illustration of the (a) best approach and (b) worst approach to minimise the burn-off to expel the interface contaminants from the weld line into the flash for Ti-6Al-4V linear friction welds [16].

- The primary reason for a Ti-6Al-4V linear friction weld being defective is due to the inclusions of contaminants, such as oxides, in the WCZ. Contaminant removal appears to be critically dependent on the processing conditions used. Larger applied pressures and smaller in-plane widths reduce the burn-off required to expel the contaminants into the flash. Interestingly, the rubbing velocity has been shown to have relatively little effect on the contaminant expulsion.
- Ti-6Al-4V linear friction welds contain residual stresses, which are primarily formed during the post-oscillatory motion cooling stage. The residual stresses can be reduced by appropriate selection of process inputs and post-weld heat treatments.
- Many of the existing methods for calculating the power input make significant assumptions, like assuming the coefficient of friction and the rubbing velocity are constant. A better way of assessing the power input and energy usage involves using the force and displacement history data from a LFW machine.
- The energy required to produce a weld is reduced with higher rubbing velocities and applied forces. This is due to these conditions reducing the overall duration of the weld and hence the energy wasted due to conduction, convection and radiation.
- There has been relatively little investigation into the clamping effects on welds. From the little data available the clamping arrangement can have a noticeable effect on the weld responses.
- Due to the rapid nature of the LFW process and the fact that the interface of the workpieces cannot be observed during welding means that using physical experiments alone may fail to provide adequate insight into the process fundamentals. Computational modelling offers a pragmatic method to understand what is happening throughout the rapidly evolving process. FEA Modelling provides an insight into many responses that are difficult to obtain experimentally, e.g. the interface contaminant removal, thermal fields and material flow. Experimental validation of models is important to ensure the accuracy of the results. Successful validation for a range of outputs allows the data predicted by the models that are non-amenable to experimental measurement to be trusted.

### *6.2. Practical implications*

Based on this review, there may be a benefit to using larger pressures and oscillating the workpieces along the shorter of the two interface-contact dimensions when producing Ti-6Al-4V welds, as shown in Fig. 30. This is because the burn-off required to remove the interface contaminants is reduced. Hence for the same burn-off, the factor of safety on contaminant removal is greater. Furthermore, these conditions can also reduce the interface temperature and refine the weld microstructure, which may offer additional benefits, such as reduced residual stresses [34,47,130] and improved mechanical properties [58,119,120].

### *6.3. Recommendations for further research*

Despite the recent advances in understanding of Ti-6Al-4V linear friction welding, there are still many more knowledge gaps that need addressing to aid further process understanding and industrial implementation.

Some recommended areas for further research are:

- **Microstructure Modelling:** Models could be used to investigate the impact of the processing conditions on the microstructure evolution. This would allow for the effects of the processing conditions on the allotropic phase, average grain size, grain microstructure and grain spatial distribution to be characterised for Ti-6Al-4V welds. The modelling approach implemented by Grujicic et al. [96,103] for a Carpenter Custom 465 precipitation-hardened martensitic stainless steel would be a good method to achieve this task. The results from this potential study could help to add some conclusive arguments to the processing condition effects on the microstructure of Ti-6Al-4V linear friction welds. Modelling could also help to identify the reasons for the different texture formations.
- **LFW Machine Effects:** The effects of the LFW machine on the welds could be investigated. This could help to answer some fundamental questions. For example, what is the most efficient way to apply the applied pressure, should it be ramped up to the maximum value quickly or slowly? Is a sinusoidal wave the best method to apply the oscillatory motion or are there better alternatives? What effect does the workpiece clamping have on the flash formation and interface contaminant expulsion? Answers to these questions would help to optimise the process.
- **Geometric Effects:** In addition to joining workpieces with a single welded surface, as has occurred for most LFW investigations, further research could address the joining of non-planar surfaces, such as "keystone" workpieces. The investigations could identify the best way to join these parts and to determine if the microstructure and properties are equal across all of the welded surfaces. Further research into joining coupons to plate could also be performed to optimise the weld contaminant removal, microstructure and properties.
- **Residual Stress Investigation:** Experiments and models could be used to investigate the impact of the processing conditions, such as the workpiece geometry, rubbing velocity and forging pressure, on the formation and magnitude of residual stresses in linear friction welds. The effectiveness of post-weld heat-treatment on the reduction of the residual stresses could also be considered. Moreover, research on steel workpieces showed that the heat in the flash refluxes back into the weld interface during the post-oscillatory cooling [153]. Further research could consider how this phenomenon affects the residual stresses in Ti-6Al-4V welds.
- **Extension to other materials:** Although the focus of this article is on Ti-6Al-4V, there is still a need to understand the effects of the LFW process on the joining of other high-value materials, such as aluminium alloys, aluminium-lithium alloys and nickel-based superalloys. A buy-to-fly ratio reduction for components made of these materials would potentially yield significant cost savings to manufacturers.

## Disclosure statement

The authors declare that there is no conflict of interest regarding the publication of this paper.

## Data access

No new data were collected in the course of this research.

## Funding

The authors would like to thank the Engineering and Physical Sciences Research Council (EPSRC), The Boeing Company, Honeywell International Inc. and The Welding Institute (TWI Ltd.) for funding the work presented in this article.

## References

[1] Addison AC. Linear friction welding information for production engineering. TWI industrial members report - 961/2010. Cambridge, U.K; 2010.
[2] Addison AC. Linear friction welding of engineering metals. TWI industrial members report - 894/2008. Cambridge, U.K.; 2008.
[3] Vairis A, Frost M. High frequency linear friction welding of a titanium alloy. Wear 1998;217:117–31. doi: https://doi.org/10.1016/S0043-1648(98)00145-8.
[4] García AMM. BLISK fabrication by linear friction welding. In: Benini E, editor. Adv Gas Turbine Technol. Winchester: InTech; 2011. p. 411–34.
[5] Chamanfar A, Jahazi M, Gholipour J, Wanjara P, Yue S. Maximizing the integrity of linear friction welded Waspaloy. Mater Sci Eng A 2012;555:117–30. doi: https://doi.org/10.1016/j.msea.2012.06.041.
[6] Wanjara P, Jahazi M. Linear friction welding of Ti-6Al-4V: processing, microstructure, and mechanical-property inter-relationships. Metall Mater Trans A 2005;36:2149–64. doi: https://doi.org/10.1007/s11661-005-0335-5.
[7] Turner R, Gebelin J-C, Ward RM, Reed RC. Linear friction welding of Ti-6Al-4V: modelling and validation. Acta Mater 2011;59:3792–803. doi: https://doi.org/10.1016/j.actamat.2011.02.028.
[8] Bhamji I, Preuss M, Threadgill PL, Addison AC. Solid state joining of metals by linear friction welding: a literature review. Mater Sci Technol 2011;27:2–12. doi: https://doi.org/10.1179/026708310X520510.
[9] Baeslack III WA, Broderick TF, Juhas M, Fraser HL. Characterization of solid-phase welds between Ti-6A1-2Sn-4Zr-2Mo-0.1Si and Ti-13.5A1-21.5Nb titanium aluminide. Mater Charact 1994;33:357–67. doi: https://doi.org/10.1016/1044-5803(94)90140-6.
[10] Maalekian M. Friction welding - critical assessment of literature. Sci Technol Weld Join 2007;12:738–58. doi: https://doi.org/10.1179/174329307X249333.
[11] Uday MB, Ahmad Fauzi MN, Zuhailawati H, Ismail aB. Advances in friction welding process: a review. Sci Technol Weld Join 2010;15:534–58. doi: https://doi.org/10.1179/136217110X12785889550064.

[12] Chamanfar A, Jahazi M, Cormier J. A review on inertia and linear friction welding of Ni-based superalloys. Metall Mater Trans A 2015;46:1639–69. doi: https://doi.org/10.1007/s11661-015-2752-4.
[13] McAndrew AR, Colegrove PA, Addison AC, Flipo BCD, Russell MJ, Lee LA. Modelling of the workpiece geometry effects on Ti-6Al-4V linear friction welds. Mater Des 2015;87:1087–99. doi: https://doi.org/10.1016/j.matdes.2015.09.080.
[14] McAndrew AR, Colegrove PA, Addison AC, Flipo BCD, Russell MJ. Modelling the influence of the process inputs on the removal of surface contaminants from Ti-6Al-4V linear friction welds. Mater Des 2015;66:183–95. doi: https://doi.org/10.1016/j.matdes.2014.10.058.
[15] McAndrew AR, Colegrove PA, Addison AC, Flipo BCD, Russell MJ. Energy and force analysis of Ti-6Al-4V linear friction welds for computational modeling input and validation data. Metall Mater Trans A 2014;45:6118–28. doi: https://doi.org/10.1007/s11661-014-2575-8.
[16] McAndrew AR. Modelling of Ti-6Al-4V linear friction welds PhD Thesis. Cranfield University; 2015.
[17] Guo Y, Jung T, Lung Y, Li H, Bray S, Bowen P. Microstructure and microhardness of Ti6246 linear friction weld. Mater Sci Eng A 2013;562:17–24. doi: https://doi.org/10.1016/j.msea.2012.10.089.
[18] Karadge M, Preuss M, Lovell C, Withers PJ, Bray S. Texture development in Ti–6Al–4V linear friction welds. Mater Sci Eng A 2007;459:182–91. doi: https://doi.org/10.1016/j.msea.2006.12.095.
[19] Guo Y, Chiu Y, Attallah M, Li H. Characterization of dissimilar linear friction welds of alpha + beta titanium alloys. J Mater Eng Perform 2012;21:770–6. doi: https://doi.org/10.1007/s11665-012-0129-z ?ASM.
[20] Martina F. Control of geometry, microstructure and mechanical properties in titanium large scale wire+arc additive manufacturing PhD Thesis. Cranfield University; 2014.
[21] Nearnetshape.co.uk. Near Net Shape (TiFab Project); 2016. <http://www.nearnetshape.co.uk/index.php/tifab-project>.
[22] Flipo B, Beamish K, Humphreys B, Wood M. Linear friction welding of Ti 6Al 4V for aerostructure applications. Trends Weld. Res. Proc. 10th Int. Conf., Tokyo, Japan; 11–14 October 2016.
[23] Allen J. An investigation into the comparative costs of additive manufacture vs. machine from solid for aero engine parts. Cost Eff. Manuf. via Net-Shape Process., Neuilly-Sur-Seine, France; 2006. p. 17–1 – 17–10.
[24] Lee LA, McAndrew AR, Buhr C, Beamish KA, Colegrove PA. 2D linear friction weld modelling of a Ti-6Al-4V T-joint. J Eng Sci Technol Rev 2015;8:44–8.
[25] Flipo B. Near-net-shape manufacturing by linear friction welding near net shape manufacturing by LFW. Sorrento, Italy: Titan. Eur.; 2014.
[26] TWI Ltd. Linear Friction Welding; 2016. <http://www.twi-global.com/capabilities/joining-technologies/friction-processes/linear-friction-welding/>.
[27] Li W, Vairis A, Preuss M, Ma T. Linear and rotary friction welding review. Int Mater Rev 2016;61:71–100. doi: https://doi.org/10.1080/09506608.2015.1109214.
[28] Vill VI. Friction welding of metals. New York: American Welding Society; 1962.
[29] Koo HH, Baeslack III WA. Structure, properties, and fracture of linear friction welded Al-Fe-V-Si alloy 8009. Mater Charact 1992;28:157–64.
[30] Garton JHL. Investigation into linear friction welding of blisks BEng Thesis. University of Bristol; 1987.
[31] Vairis A, Frost M. On the extrusion stage of linear friction welding of Ti-6Al-4V. Mater Sci Eng A 1999;271:477–84. doi: https://doi.org/10.1016/S0921-5093(99)00449-9.
[32] Vairis A, Frost M. Modelling the linear friction welding of titanium blocks. Mater Sci Eng A 2000;292:8–17. doi: https://doi.org/10.1016/S0921-5093(00)01036-4.
[33] Vairis A. High frequency linear friction welding PhD Thesis. University of Bristol; 1998.
[34] Romero J, Attallah MM, Preuss M, Karadge M, Bray SE. Effect of the forging pressure on the microstructure and residual stress development in Ti–6Al–4V linear friction welds. Acta Mater 2009;57:5582–92. doi: https://doi.org/10.1016/j.actamat.2009.07.055.
[35] Ma TJ, Li W-Y, Yang SY. Impact toughness and fracture analysis of linear friction welded Ti–6Al–4V alloy joints. Mater Des 2009;30:2128–32. doi: https://doi.org/10.1016/j.matdes.2008.08.029.
[36] Mary C, Jahazi M. Multi-scale analysis of IN-718 microstructure evolution during linear friction welding. Adv Eng Mater 2008;10:573–8. doi: https://doi.org/10.1002/adem.200700361.
[37] Jun T-S, Rotundo F, Song X, Ceschini L, Korsunsky AM. Residual strains in AA2024/AlSiCp composite linear friction welds. Mater Des 2010;31:S117–20. doi: https://doi.org/10.1016/j.matdes.2009.10.004.
[38] Rotundo F, Ceschini L, Morri A, Jun T-S, Korsunsky AM. Mechanical and microstructural characterization of 2124Al/25vol.%SiCp joints obtained by linear friction welding (LFW). Compos Part A Appl Sci Manuf 2010;41:1028–37. doi: https://doi.org/10.1016/j.compositesa.2010.03.009.
[39] Lang B, Zhang TC, Li XH, Guo DL. Microstructural evolution of a TC11 titanium alloy during linear friction welding. J Mater Sci 2010;45:6218–24. doi: https://doi.org/10.1007/s10853-010-4716-9.
[40] Bhamji I, Preuss M, Threadgill PL, Moat RJ, Addison AC, Peel MJ. Linear friction welding of AISI 316L stainless steel. Mater Sci Eng A 2010;528:680–90. doi: https://doi.org/10.1016/j.msea.2010.09.043.
[41] Ma T, Chen T, Li W-Y, Wang S, Yang S. Formation mechanism of linear friction welded Ti–6Al–4V alloy joint based on microstructure observation. Mater Charact 2011;62:130–5. doi: https://doi.org/10.1016/j.matchar.2010.11.009.
[42] Ma TJ, Zhong B, Li W-Y, Zhang Y, Yang S, Yang C. On microstructure and mechanical properties of linear friction welded dissimilar Ti-6Al-4V and Ti-6 5Al-3 5Mo-1 5Zr-0 3Si joint. Sci Technol Weld Join 2012;17:9–12. doi: https://doi.org/10.1179/1362171811Y.0000000067.
[43] Bhamji I, Moat RJ, Preuss M, Threadgill PL, Addison AC, Peel MJ. Linear friction welding of aluminium to copper. Sci Technol Weld Join 2012;17:314–20. doi: https://doi.org/10.1179/1362171812Y.0000000010.
[44] Li W, Wu H, Ma T, Yang C, Chen Z. Influence of parent metal microstructure and post-weld heat treatment on microstructure and mechanical properties of linear friction welded Ti-6Al-4V joint. Adv Eng Mater 2012;14:312–8. doi: https://doi.org/10.1002/adem.201100203 Influence.
[45] Bhamji I, Preuss M, Moat RJ, Threadgill PL, Addison AC. Linear friction welding of aluminium to magnesium. Sci Technol Weld Join 2012;17:368–74. doi: https://doi.org/10.1179/1362171812Y.0000000017.
[46] Schroeder F, Ward RM, Turner RP, Attallah MM, Gebelin J, Reed RC. Linear friction welding of titanium alloys for aeroengine applications: modelling and validation. In: 9th Int. Conf. Trends Weld. Res., Chicago, USA; 2012. p. 886–92.
[47] Turner R, Ward RM, March R, Reed RC. The magnitude and origin of residual stress in Ti-6Al-4V linear friction welds: an investigation by validated numerical modeling. Metall Mater Trans B 2012;43:186–97. doi: https://doi.org/10.1007/s11663-011-9563-9.
[48] Li W, Ma T, Li J. Numerical simulation of linear friction welding of titanium alloy: effects of processing parameters. Mater Des 2010;31:1497–507. doi: https://doi.org/10.1016/j.matdes.2009.08.023.
[49] Ofem UU, Colegrove PA, Addison A, Russell MJ. Energy and force analysis of linear friction welds in medium carbon steel. Sci Technol Weld Join 2010;15:479–85. doi: https://doi.org/10.1179/136217110X12731414739790.
[50] Romilly P. Linear friction welding for near net shape manufacturing of titanium parts. In: Venkatesh V, Pilchak AL, Allison JE, Ankem S, Boyer R, Christodoulou J, et al., editors. Proc. 13th World Conf. Titan., San Diego, California, USA: The Minerals, Metals & Materials Society; 2016. p. 1423–7. doi:https://doi.org/10.1002/9781119296126.
[51] Daymond MR, Bonner NW. Measurement of strain in a titanium linear friction weld by neutron diffraction. Physica B 2003;325:130–7. doi: https://doi.org/10.1016/S0921-4526(02)01514-4.
[52] Ceretti E, Fratini L, Giardini C, Spisa D. Numerical modelling of the linear friction welding process. Int J Mater Form 2010;3:1015–8. doi: https://doi.org/10.1007/s12289-010-0942-6.
[53] Li W, Ma T, Zhang Y, Xu Q, Li J, Yang S, et al. Microstructure characterization and mechanical properties of linear friction welded Ti-6Al-4V alloy. Adv Eng Mater 2008;10:89–92. doi: https://doi.org/10.1002/adem.200700034.
[54] Ma TJ, Li WY, Zhong B, Zhang Y, Li JL. Effect of post-weld heat treatment on microstructure and property of linear friction welded Ti17 titanium alloy joint. Sci Technol Weld Join 2012;17:180–5. doi: https://doi.org/10.1179/1362171811Y.0000000079.

[55] Sorina-Müller J, Rettenmayr M, Schneefeld D, Roder O, Fried W. FEM simulation of the linear friction welding of titanium alloys. Comput Mater Sci 2010;48:749–58. doi: https://doi.org/10.1016/j.commatsci.2010.03.026.
[56] Corzo V, Casals O, Alcalá J, Mateo A, Anglada M. Mechanical evaluation of linear friction welds in titanium alloys through indentation experiments. Weld Int 2007;21:125–9. doi: https://doi.org/10.1533/wint.2007.3723.
[57] Rotundo F, Marconi A, Morri A, Ceschini A. Dissimilar linear friction welding between a SiC particle reinforced aluminum composite and a monolithic aluminum alloy: Microstructural, tensile and fatigue properties. Mater Sci Eng A 2013;559:852–60. doi: https://doi.org/10.1016/j.msea.2012.09.033.
[58] Grujicic M, Arakere G, Pandurangan B, Yen CF, Cheeseman BA. Process modeling of Ti-6Al-4V linear friction welding (LFW). J Mater Eng Perform 2011;21:2011–23. doi: https://doi.org/10.1007/s11665-011-0097-8 ?ASM.
[59] Xie MY, Jun TS, Korsunsky AM, Drakopoulos M. Analysis of preferred orientations in linear friction welded (LFW) aluminium alloy specimens using "one-shot" multi-element energy dispersive synchrotron X-ray diffraction. Powder Diffr 2013;28:327–32. doi: https://doi.org/10.1017/S0885715613000948.
[60] Chamanfar A, Jahazi M, Gholipour J, Wanjara P, Yue S. Mechanical property and microstructure of linear friction welded WASPALOY. Metall Mater Trans A 2010;42:729–44. doi: https://doi.org/10.1007/s11661-010-0457-2.
[61] Wanjara P, Dalgaard E, Trigo G, Mandache C, Comeau G, Jonas JJ. Linear friction welding of Al-Cu: Part 1 - Process evaluation. Can Metall Q 2011;50:350–9. doi: https://doi.org/10.1179/000844311X13112418194644.
[62] Bergmann JP, Petzoldt F, Schürer R, Schneider S. Solid-state welding of aluminum to copper—case studies. Weld World 2013;57:541–50. doi: https://doi.org/10.1007/s40194-013-0049-z.
[63] Dalgaard E, Wanjara P, Trigo G, Jahazi M, Comeau G, Jonas JJ. Linear friction welding of Al-Cu part 2 - Interfacial characteristics. Can Metall Q 2011;50:360–70. doi: https://doi.org/10.1179/000844311X13112418194671.
[64] Bhandari V. Linear friction welding of titanium to stainless steel (MSc Thesis). Cranfield University; 2010.
[65] Bhamji IM. Development of the linear friction welding process EngD Thesis. University of Manchester; 2012.
[66] Leyens C, Peters M. Titanium and titanium alloys: fundamentals and applications. 1st ed. Darmstadt: Wiley-VCH; 2003.
[67] Shtrikman MM. Linear friction welding. Weld Int 2010;24:563–9. doi: https://doi.org/10.1080/09507110903569149.
[68] Kallee SW, Nicholas ED, Russell MJ. Friction welding of aero engine components. In: Lutjering G, Albrecht J, editors. 10th world Conf. Titan. TI-2003. Hamburg, Germany: Wiley-VCH; 2003. p. 2867–74.
[69] Lütjering G, Williams JC. Titanium. 2nd ed. Berlin Heidelberg New York: Springer; 2007.
[70] Frankel P, Preuss M, Steuwer A, Withers PJ, Bray S. Comparison of residual stresses in Ti–6Al–4V and Ti–6Al–2Sn–4Zr–2Mo linear friction welds. Mater Sci Technol 2009;25:640–50. doi: https://doi.org/10.1179/174328408X332825.
[71] Corzo M, Torres Y, Anglada M, Mateo A. Fracture behaviour of linear friction welds in titanium alloys. An La Mecánica Fract 2007;1:75–80.
[72] Ji Y, Chai Z, Zhao D, Wu S. Linear friction welding of Ti–5Al–2Sn–2Zr–4Mo–4Cr alloy with dissimilar microstructure. J Mater Process Technol 2014;214:979–87. doi: https://doi.org/10.1016/j.jmatprotec.2013.11.006.
[73] Sadallah Y. Linear friction welding - aero structure parts (ACB Presentation). In: 4th Linear Frict. Weld. Symp., Granta Park, Cambridge, U.K.; 2017.
[74] Piolle N. Linear Friction Welding - General Presentation (ACB Presentation). In: 4th Linear Frict. Weld. Symp., Granta Park, Cambridge, U.K.; 2017.
[75] Slattery KT. Structural assemblies and preforms therefor formed by linear friction welding. US7225967; 2007.
[76] Effertz PS, Fuchs F, Enzinger N. Modelling the flash formation of linear friction welded 30CrNiMo8 high strength steel chains. Int J Adv Manuf Technol; 2017 doi:https://doi.org/10.1007/s00170-017-0338-6 [in press].
[77] Brian M, Harris T. How caterpillar backhoe loaders work (Howstuffworks.com); 2001. <http://science.howstuffworks.com/transport/engines-equipment/backhoe-loader4.htm> [accessed March 27, 2014].
[78] Kuroki H, Nezaki K, Wakabayashi T, Nakamura K. Application of linear friction welding technique to aircraft engine parts. IHI Eng Rev 2014;47:40–3.
[79] Shilton A. Economic Assessment of LFW (Ten Solutions Presentation). In: 4th Linear Frict. Weld. Symp., Granta Park, Cambridge, U.K.; 2017.
[80] Moody SM, Atkinson JR. Linear friction welding of polypropylene and polycarbonate. Part II. The microstructures and mechanical properties of PP welds made using optimum conditions. Plast Rubber Compos Process Appl 1992;17:211–7.
[81] Moody SM, Atkinson JR. Linear friction welding of polypropylene and polycarbonate. Part I. Effects of welding conditions on strength of welds. Plast Rubber Compos Process Appl 1992;17:203–9.
[82] Vaziri M, Lindgren O, Pizzi A. Influence of machine setting and wood parameters on crack formation in scots pine joints produced by linear friction welding. J Adhes Sci Technol 2012;26:37–41. doi: https://doi.org/10.1163/156856111X610126.
[83] Vaziri M, Berg S, Sandberg D, Gheinani IT. Three-dimensional finite element modelling of heat transfer for linear friction welding of scots pine. Wood Mater Sci Eng 2014:1–8. doi: https://doi.org/10.1080/17480272.2014.903297.
[84] Chamanfar A, Sarrat L, Jahazi M, Asadi M, Weck A, Koul AK. Microstructural characteristics of forged and heat treated Inconel-718 disks. Mater Des 2013;52:791–800. doi: https://doi.org/10.1016/j.matdes.2013.06.004.
[85] Ola OT, Ojo OA, Wanjara P, Chaturvedi MC. A study of linear friction weld microstructure in single crystal CMSX-486 superalloy. Metall Mater Trans A 2011;43:921–33. doi: https://doi.org/10.1007/s11661-011-0928-0.
[86] Karadge M, Preuss M, Withers PJ, Bray S. Importance of crystal orientation in linear friction joining of single crystal to polycrystalline nickel-based superalloys. Mater Sci Eng A 2008;491:446–53. doi: https://doi.org/10.1016/j.msea.2008.04.064.
[87] Chamanfar A, Jahazi M, Gholipour J, Wanjara P, Yue S. Modeling grain size and strain rate in linear friction welded waspaloy. Metall Mater Trans A 2013;44:4230–8. doi: https://doi.org/10.1007/s11661-013-1767-y.
[88] Ola OT, Ojo OA, Wanjara P, Chaturvedi MC. Enhanced resistance to weld cracking by strain-induced rapid solidification during linear friction welding. Philos Mag Lett 2011;91:140–9. doi: https://doi.org/10.1080/09500839.2010.541164.
[89] Vishwakarma KR, Ojo OA, Wanjara P, Chaturvedi MC. Microstructural analysis of linear friction-welded 718 plus superalloy. J Miner Met Mater Soc 2014;66:2525–34. doi: https://doi.org/10.1007/s11837-014-0938-7.
[90] Chamanfar A, Jahazi M, Gholipour J, Wanjara P, Yue S. Suppressed liquation and microcracking in linear friction welded WASPALOY. Mater Des 2012;36:113–22. doi: https://doi.org/10.1016/j.matdes.2011.11.007.
[91] Amegadzie MY, Ola OT, Ojo OA, Wanjara P, Chaturvedi MC. On liquidation and liquid phase oxidation during linear friction welding of nickel-base IN 738and CMSX 486 superalloys. In: Huron ES, Reed RC, Hardy MC, Mills MJ, Montero RE, Portella PD, et al., editors. Superalloys 2012 12"' Int. Symp. Superalloys, Champion, Pennsylvania, USA: The Minerals, Metals & Materials Society; 2012. p. 587–94.
[92] Fratini L, Buffa G, Cammalleri M, Campanella D. On the linear friction welding process of aluminum alloys: experimental insights through process monitoring. CIRP Ann - Manuf Technol 2013;62:295–8. doi: https://doi.org/10.1016/j.cirp.2013.03.056.
[93] Song X, Xie M, Hofmann F, Jun TS, Connolley T, Reinhard C, et al. Residual stresses in linear friction welding of aluminium alloys. Mater Des 2013;50:360–9. doi: https://doi.org/10.1016/j.matdes.2013.03.051.
[94] Ma TJ, Li W-Y, Xu QZ, Zhang Y, Li JL, Yang SQ, et al. Microstructure evolution and mechanical properties of linear friction welded 45 steel joint. Adv Eng Mater 2007;9:703–7. doi: https://doi.org/10.1002/adem.200700090.
[95] Fratini L, Buffa G, Campanella D, La Spisa D. Investigations on the linear friction welding process through numerical simulations and experiments. Mater Des 2012;40:285–91. doi: https://doi.org/10.1016/j.matdes.2012.03.058.
[96] Grujicic M, Yavari R, Snipes JS, Ramaswami S, Yen C-F, Cheeseman BA. Linear friction welding process model for carpenter custom 465 precipitation-hardened martensitic stainless steel. J Mater Eng Perform 2014;23:2182–98. doi: https://doi.org/10.1007/s11665-014-0985-9.
[97] Dalgaard EC. Evolution of microstructure, microtexture and mechanical properties in linear friction welded titanium alloys PhD Thesis. McGill University; 2011.
[98] Li W, Wang F, Shi S, Ma T, Li J, Vairis A. 3D finite element analysis of the effect of process parameters on linear friction welding of mild steel. J Mater Eng Perform 2014;23:4010–8. doi: https://doi.org/10.1007/s11665-014-1197-z.

[99] Ma TJ, Chen X, Li WY, Yang XW, Zhang Y, Yang SQ. Microstructure and mechanical property of linear friction welded nickel-based superalloy joint. Mater Des 2016;89:85–93. doi: https://doi.org/10.1016/j.matdes.2015.09.143.
[100] Chen X, Xie FQ, Ma TJ, Li WY, Wu XQ. Microstructure evolution and mechanical properties of linear friction welded Ti2AlNb alloy. J Alloys Compd 2015;646:490–6. doi: https://doi.org/10.1016/j.jallcom.2015.05.198.
[101] Avettand-Fènoël M-N, Racineux G, Debeugny L, Taillard R. Microstructural characterization and mechanical performance of an AA2024 aluminium alloy — pure copper joint obtained by linear friction welding. Mater Des 2016;98:305–18. doi: https://doi.org/10.1016/j.matdes.2016.03.029.
[102] Astarita A, Scherillo F, Curioni M, Aprea P, Impero F, Squillace A, et al. Study of the Linear Friction Welding process of dissimilar Ti-6Al-4V – stainless steel joints. Mater Manuf Process; 2016, doi: https://doi.org/10.1080/10426914.2016.1151048.
[103] Grujicic M, Yavari R, Snipes JS, Ramaswami S. A linear friction welding process model for Carpenter Custom 465 precipitation-hardened martensitic stainless steel: a weld microstructure- evolution analysis. J Eng Manuf 2015;229:1997–2020. doi: https://doi.org/10.1177/0954405414542137.
[104] Pederson R. Microstructure and phase transformation of Ti-6Al-4V PhD Thesis. Luleå University of Technology; 2002.
[105] Charles C. Modelling microstructure evolution of weld deposited Ti-6Al-4V PhD Thesis. Luleå University of Technology; 2008.
[106] Henry SD, Reidenbach F. Fatigue data book - light structural alloys. ASM International; 1994.
[107] Dewald AT, Legzdina D, Clausen B, Brown DW, Sisneros TA, Hill MR. A comparison of residual stress measurements on a linear friction weld using the contour method and neutron diffraction. Conf Proc Soc Exp Mech Ser 2013;4:183–9. doi: https://doi.org/10.1007/978-1-4614-4226-4.
[108] Schröder F, Ward RM, Walpole AR, Turner RP, Attallah MM, Gebelin J-C, et al. Linear friction welding of Ti6Al4V: experiments and modelling. Mater Sci Technol 2015;31:372–84. doi: https://doi.org/10.1179/1743284714Y.0000000575.
[109] Stinville JC, Bridier F, Ponsen D, Wanjara P, Bocher P. High and low cycle fatigue behavior of linear friction welded Ti–6Al–4V. Int J Fatigue 2015;70:278–88. doi: https://doi.org/10.1016/j.ijfatigue.2014.10.002.
[110] Attallah MM, Preuss M, Bray S. Microstructural development during Linear friction welding of titanium alloys. In: 8th Int. Conf. Trends Weld. Res., Pine Mountain, GA; United States; 2009. p. 486–91. doi:https://doi.org/10.1361/cp2008twr486.
[111] Ding R, Guo ZX, Wilson A. Microstructural evolution of a Ti–6Al–4V alloy during thermomechanical processing. Mater Sci Eng A 2002;327:233–45. doi: https://doi.org/10.1016/S0921-5093(01)01531-3.
[112] Seshacharyulu T, Medeiros SC, Frazier WG, Prasad YVRK. Microstructural mechanisms during hot working of commercial grade Ti – 6Al – 4V with lamellar starting structure. Mater Sci Eng A 2002;325:112–25. doi: https://doi.org/10.1016/S0921-5093(01)01448-4.
[113] Buffa G, Campanella D, Cammalleri M, Ducato A, Astarita A, Squillace A, et al. Experimental and numerical analysis of microstructure evolution during linear friction welding of Ti6Al4V. Proc Manuf 2015;1:429–41. doi: https://doi.org/10.1016/j.promfg.2015.09.053.
[114] Ahmed T, Rack HJ. Phase transformations during cooling in α+β titanium alloys. Mater Sci Eng A 1998;243:206–11. doi: https://doi.org/10.1016/S0921-5093(97)00802-2.
[115] Seshacharyulu T, Medeiros SC, Frazier WG, Prasad YVRK. Hot working of commercial Ti-6Al-4V with an equiaxed alpha-beta microstructure: materials modeling considerations. Mater Sci Eng A 2000;284:184–94. doi: https://doi.org/10.1016/S1359-6462(99)00163-3.
[116] Schroeder F, Ward RM, Turner RP, Walpole AR, Attallah MM, Gebelin J-C, et al. Validation of a model of linear friction welding of Ti6Al4V by considering welds of different sizes. Metall Mater Trans B 2015;46:2326–31. doi: https://doi.org/10.1007/s11663-015-0396-9.
[117] McAndrew AR, Bühr C, Flipo BCD, Colegrove PA. 3D modelling of Ti-6Al-4V linear friction welds. Sci Technol Weld Join 2016;22:496–504. doi: https://doi.org/10.1080/13621718.2016.1263439.
[118] Gil FJ, Ginebra MP, Manero JM, Planell JA. Formation of alpha-Widmanstatten structure: effects of grain size and cooling rate on the Widmanstatten morphologies and on the mechanical properties in Ti6Al4V alloy. J Alloys Compd 2001;329:142–52. doi: https://doi.org/10.1016/S0925-8388(01)01571-7.
[119] Zhang Y, Sato YS, Kokawa H, Park SHC, Hirano S. Microstructural characteristics and mechanical properties of Ti–6Al–4V friction stir welds. Mater Sci Eng A 2008;485:448–55. doi: https://doi.org/10.1016/j.msea.2007.08.051.
[120] Lütjering G. Influence of processing on microstructure and mechanical properties of (alpha + beta) titanium alloys. J Alloys Compd 1998;243:32–45. doi: https://doi.org/10.1016/S0921-5093(97)00778-8.
[121] Bikmeyev AT, Gazizov RK, Vairis A, Yamileva AM. Modelling the temperature distribution in the contact area of a moving object in the case of linear friction welding. In: Proc. ASME 2013 Int. Mech. Eng. Congr. Expo. IMECE2013, San Diego, California, U.S.A.: ASME; 2013. p. 1–8, doi:https://doi.org/10.1115/IMECE2013-64343.
[122] Li W, Guo J, Yang X, Vairis A. The effect of micro-swinging on joint formation in linear friction welding. J Eng Sci Technol Rev 2014;7:55–8.
[123] Astarita A, Coppola M, Esposito S, Liberini M, Maio L, Papa I, et al. Experimental characterization of Ti6Al4V T joints welded through linear friction welding technique: microstructure and NDE. Adv Manuf; 2016. doi:https://doi.org/10.1007/s40436-016-0160-7 [in press].
[124] Guo Y, Attallah MM, Chiu Y, Li H, Bray S, Bowen P. Spatial variation of microtexture in linear friction welded Ti-6Al-4V. Mater Charact; 2017, doi: https://doi.org/10.1016/j.matchar.2017.03.019.
[125] Wen GD, Ma TJ, Li WY, Li JL, Guo HZ, Chen DL. Cyclic deformation behavior of linear friction welded Ti6Al4V joints. Mater Sci Eng A 2014;597:408–14. doi: https://doi.org/10.1016/j.msea.2014.01.006.
[126] Flipo B. Ti-6Al-4V LFW for aero structures. In: 4th Linear Frict. Weld. Symp., Granta Park, Cambridge, U.K.; 2017.
[127] Suleimanova GR, Kabirov RR, Karavaeva MV, Ershova YA, Zhilyaev AP. Investigation of torsional strength of the VT6 weld joint produced by linear friction welding. Russ Phys J 2015;58:67–73. doi: https://doi.org/10.1007/s11182-015-0574-x.
[128] Stachowiak GW, Batchelor AW. Engineering tribology. 2nd ed. Oxford, U.K.: Butterworth-Heinemann; 2000.
[129] Askeland D, Phule P. The science and engineering of materials. 5th ed. London: Thomson; 2006.
[130] Nikiforov R, Medvedev A, Tarasenko E, Vairis A. Numerical simulation of residual stresses in linear friction welded joints. J Eng Sci Technol Rev 2015;8:49–53.
[131] Bühr C, McAndrew AR, Colegrove PA, Lee LA, Flipo BCD, Russell MJ. An innovative approach for modelling residual stresses in Ti-6Al-4V linear friction welds. In: Sommitsch C, Enzinger N, Mayr P, Sommitsch C, Enzinger N, Mayr P, editors. 11th Int. Semin. Numer. Anal. Weldability (Mathematical Model. Weld Phenom. 11). Schloss Seggau, Graz, Austria: The Institute for Materials Science and Welding (IWS) at Graz University of Technology; 2015. p. 549–64.
[132] Fu Y, Li W-Y, Yang X-W, Ma T-J, Vairis A. The effects of forging pressure and temperature field on residual stresses in linear friction welded Ti6Al4V joints. Adv Manuf; 2016, doi:https://doi.org/10.1007/s40436-016-0161-6 [in press].
[133] Jones S. Low Force Friction (Linear) Welding (MTI Presentation). In: 4th Linear Frict. Weld. Symp., Granta Park, Cambridge, U.K.; 2017.
[134] Yamileva AM, Gazizov RK, Vairis A. Computer modelling of the effect of clamping in linear friction welding. J Eng Sci Technol Rev 2015;8:65–8.
[135] Vairis A, Christakis N. The development of a continuum framework for friction welding processes with the aid of micro-mechanical parameterisations. Int J Model Identif Control 2007;2:347–55. doi: https://doi.org/10.1504/IJMIC.2007.016417.
[136] Reilly A. Modelling of friction stir spot welding (PhD Thesis). Cambridge University; 2013.
[137] Cozzolino LD. Finite element analysis of localised rolling to reduce residual stress and distortion PhD Thesis. Cranfield University; 2014.
[138] Vairis A. Mathematical modelling of the linear friction welding process. J Eng Sci Technol Rev 2012;5:25–31.
[139] Lacey AA, Voong C. Transient thermal behaviour in a model of linear friction welding. J Eng Math 2013. doi: https://doi.org/10.1007/s10665-013-9650-9.
[140] Kavallaris NI, Lacey AA, Nikolopoulos CV, Voong C. Behaviour of a non-local equation modelling linear friction welding. Appl Math 2007;72:597–616. doi: https://doi.org/10.1093/imamat/hxm031.
[141] Carslaw HS, Jaeger JC. Conduction of heat in solids. 2nd ed. Oxford, England: Oxford University Press; 1959.
[142] Yang L. Modelling of the inertia welding of inconel 718 PhD Thesis. University of Birmingham; 2010.
[143] Lindgren L-E. Numerical modelling of welding. Comput Methods Appl Mech Eng 2006;195:6710–36. doi: https://doi.org/10.1016/j.cma.2005.08.018.

[144] Turner R, Schroeder F, Ward RM, Brooks JW. The importance of materials data and modelling parameters in an FE simulation of linear friction welding. Adv Mater Sci Eng 2014;2014:1–8. doi: https://doi.org/10.1155/2014/521937.
[145] Bikmeyev A, Gazizov RK, Yamileva AM, Vairis A, Zheleznov FO. On the visualization of joint formation during linear friction welding. J Eng Sci Technol Rev 2015;8:69–72.
[146] Bychkov V, Medvedev A, Pautov A. Computer modeling in the design of the blade blank for linear friction welding. J Eng Sci Technol Rev 2014;7:62–5.
[147] Kiselyeva SK, Yamileva AM, Karavaeva MV, Nasibullayev IS, Bychkov VM, Medvedev AY, et al. Computer modelling of linear friction welding based on the joint microstructure. J Eng Sci Technol Rev 2012;5:44–7.
[148] Li W, Guo J, Ma T, Vairis A. Numerical modeling of linear friction welding: a literature review. China Weld 2015;23:1–7.
[149] Li W, Wang F, Shi S, Ma T. Numerical simulation of linear friction welding based on ABAQUS environment: Challenges and perspectives. J Mater Eng Perform 2014;23:384–90. doi: https://doi.org/10.1007/s11665-013-0776-8.
[150] Tao J, Zhang T, Liu P, Li J, Mang Y. Numerical computation of a linear friction welding process. Mater Sci Forum 2008;575–578:811–5. doi: https://doi.org/10.4028/www.scientific.net/MSF.575-578.811.
[151] Yamileva AM, Selivanov AS, Gazizov RK, Vairis A. A two-parameter 2D-model of the elastic stage of linear friction welding using ANSYS mechanical finite element analysis programme. J Eng Sci Technol Rev 2012;5:6–9.
[152] Maio L, Franco F, Squillace A, Lecce L. A simplified approach to numerical simulation of LFW process of Ti6Al4V alloy: investigation on friction and temperature. Int J Adv Manuf Technol 2016;86:3217–28. doi: https://doi.org/10.1007/s00170-016-8447-1.
[153] Li W, Shi SX, Wang FF, Ma TJ, Li JL, Gao DL, et al. Heat reflux in flash and its effect on joint temperature history during linear friction welding of steel. Int J Therm Sci 2013;67:192–9. doi: https://doi.org/10.1016/j.ijthermalsci.2012.12.004.
[154] Wu X. Finite element simulation of linear friction welding. Adv Mater Res 2012;411:126–9. doi: https://doi.org/10.4028/www.scientific.net/AMR.41.126.
[155] Pashazadeh H, Teimournezhad J, Masoumi A. Numerical investigation on the mechanical, thermal, metallurgical and material flow characteristics in friction stir welding of copper sheets with experimental verification. Mater Des 2014;55:619–32. doi: https://doi.org/10.1016/j.matdes.2013.09.028.
[156] Pashazadeh H, Masoumi A, Teimournezhad J. A study on material flow pattern in friction stir welding using finite element method. Proc Inst Mech Eng Part B J Eng Manuf 2013;227:1453–66. doi: https://doi.org/10.1177/0954405413485952.
[157] Shimoda Y, Tsubaki M, Yasui T, Fukumoto M. Experimental and numerical studies of material flow during welding by friction stirring. Yosetsu Gakkai Ronbunshu/Quarterly J Japan Weld Soc 2010;29:114–8.
[158] Gao Z, Niu JT, Krumphals F, Enzinger N, Mitsche S, Sommitsch C. FE modelling of microstructure evolution during friction stir spot welding in AA6082-T6. Weld World 2013;57:895–902. doi: https://doi.org/10.1007/s40194-013-0083-x.
[159] Buffa G, Fratini L. Strategies for numerical simulation of linear friction welding of metals: a review. Prod Eng; 2017, doi:https://doi.org/10.1007/s11740-017-0726-7.
[160] Bühr C, Colegrove PA, McAndrew AR. An efficient numerical modelling approach to predict residual stresses in Ti-6Al-4V linear friction welds. In: TBC, editor. 10th Int. Conf. Trends Weld. Res., Tokyo, Japan: ASM International; 2016. p. 522–5.
[161] Liu ZM, Guo ZU, Zhao GY, Zhang S, Pan JL. 3D numerical simulation of linear friction welding of 45# carbon steel. Adv Mater Res 2012;538–541:1443–6. doi: https://doi.org/10.4028/www.scientific.net/AMR.476-478.701.
[162] Maio L, Liberini M, Campanella D, Astarita A, Esposito S, Boccardi S, et al. Infrared thermography for monitoring heat generation in a linear friction welding process of Ti6Al4V alloy. Infrared Phys Technol 2017. doi: https://doi.org/10.1016/j.infrared.2017.01.023.